

Special Section:

Ophiolites and Oceanic Lithosphere, with a focus on the Samail ophiolite in Oman

Key Points:

- Abundant cataclasites overprint previously formed listvenite in the Oman Drilling Hole BT1B
- Cataclasis was related to fluid flow, which caused Mg loss and/or Si enrichment, and local redistribution of Cr
- The multistage tectonic overprint after peridotite carbonation in the Oman ophiolite should be excluded when analyzing early structures

Supporting Information:

- Supporting Information S1

Correspondence to:

M. D. Menzel,
manuel.menzel@emr.rwth-aachen.de;
manuelmenzel@gmail.com

Citation:

Menzel, M. D., Urai, J. L., de Obeso, J. C., Kotowski, A., Manning, C. E., Kelemen, P. B., et al. (2020). Brittle deformation of carbonated peridotite—Insights from listvenites of the Samail ophiolite (Oman Drilling Project Hole BT1B). *Journal of Geophysical Research: Solid Earth*, 125, e2020JB020199. <https://doi.org/10.1029/2020JB020199>

Received 19 MAY 2020






Accepted 21 SEP 2020

Accepted article online 12 OCT 2020

©2020. The Authors.

This is an open access article under the terms of the Creative Commons Attribution-NonCommercial License, which permits use, distribution and reproduction in any medium, provided the original work is properly cited and is not used for commercial purposes.

Brittle Deformation of Carbonated Peridotite—Insights From Listvenites of the Samail Ophiolite (Oman Drilling Project Hole BT1B)

Manuel D. Menzel¹ , Janos L. Urai^{1,2} , Juan Carlos de Obeso³ , Alissa Kotowski^{4,5} , Craig E. Manning⁶, Peter B. Kelemen³, Michael Kettermann⁷ , Ana P. Jesus^{2,8}, Yumiko Harigane⁹ , and the Oman Drilling Project Phase 1 Science Team

¹Institute of Tectonics and Geodynamics, RWTH Aachen University, Aachen, Germany, ²Department of Applied Geosciences, German University of Technology (GUTech), Muscat, Oman, ³Lamont-Doherty Earth Observatory, Columbia University, Palisades, NY, USA, ⁴Department of Geological Sciences, Jackson School of Geosciences, University of Texas at Austin, Austin, TX, USA, ⁵Now at Department of Earth and Planetary Sciences, McGill University, Montreal, Quebec, Canada, ⁶Dept. of Earth & Space Sciences, University of California, Los Angeles, CA, USA, ⁷Department of Geodynamics and Sedimentology, University of Vienna, Vienna, Austria, ⁸Now at Instituto Dom Luiz (IDL), Faculdade de Ciências, Universidade de Lisboa, Lisbon, Portugal, ⁹Institute of Geology and Geoinformation, Geological Survey of Japan, National Institute of Advanced Industrial Science and Technology, Tsukuba, Japan

Abstract Hole BT1B of the Oman Drilling Project provides a continuous sampling from listvenite into the metamorphic sole that preserves the deformation, hydration, and carbonation processes of oceanic mantle peridotite at the base of the Samail ophiolite, Oman. We present evidence of multistage brittle deformation in listvenites and serpentinites based on field observations, visual core logging and petrography. About 10 vol% of listvenite and serpentinite in Hole BT1B is composed of cataclasis bands. Cataclasites contain lithic clasts of listvenite with spheroidal, zoned magnesite and quartz, and fragments of chalcedony-carbonate veins that elsewhere crosscut listvenite—showing that cataclasis postdates listvenite formation. Locally the cataclasites are reworked and cut by thin, sharp faults, pointing to repeated reactivation of brittle structures. SEM-EDS mapping shows that cataclasis was related to dissolution of carbonate and/or silica cementation. Dolomite veins crosscut cataclasites and breccias, suggesting that part of the Ca gain in BT1B is related to late fluids after listvenite formation. These results indicate a multistage tectonic overprint after peridotite carbonation and listvenite formation, which may be related to the tectonic history of the deformed continental margin under the ophiolite. These relatively late brittle structures should be excluded when trying to understand the carbonation of peridotite to listvenite.

1. Introduction

The interaction of mantle rocks with carbon-bearing aqueous fluids causes large amounts of volatiles to be stored in altered peridotite due to hydration (serpentinization) and carbonation reactions of olivine and pyroxene. These reactions are particular in that they produce very volatile-rich alteration products (up to 15 wt% H₂O or 35 wt% CO₂ in fully hydrated or carbonated peridotite, respectively), have comparatively fast reaction rates, and can pervasively transform large volumes of rock (Beinlich, John, et al., 2020; Kelemen et al., 2011). Therefore, the alteration of Mg-bearing silicates in peridotite can have a substantial impact on the global geochemical cycling of volatiles (Alt et al., 2013; Beinlich et al., 2018). In particular, peridotites in the cold part of the mantle wedge of subduction zones may take up large amounts of water and carbon during serpentinization and carbonation reactions caused by C-bearing, aqueous subduction fluids derived from the slab (Hyndman & Peacock, 2003; Kelemen & Manning, 2015). The reaction characteristics of olivine and pyroxene alteration further make exposures of peridotites in ophiolites a promising target for strategies of carbon sequestration by mineral carbonation (Kelemen et al., 2018; Kelemen & Matter, 2008; Paukert et al., 2012).

In the extreme, the interaction of peridotite with C-bearing fluid produces listvenite, a rock where all Mg-bearing silicates are replaced by carbonate and quartz, and relict chromian spinel is partly transformed into chromian mica (fuchsite-muscovite solid solutions) (Halls & Zhao, 1995). Listvenites often are associated with talc-carbonate assemblages (soapstone) and carbonate-bearing serpentinites, which form at different fluid/rock ratios during the interaction of peridotite with C-bearing aqueous fluids

(Beinlich et al., 2012; Hansen et al., 2005; Menzel et al., 2018). Because serpentinized peridotites have low Ca contents, carbonates in listvenites are typically magnesite and minor dolomite. C-bearing fluids are commonly interpreted to be derived from underlying carbonate-bearing metasediment. Locally, listvenites can be associated with birbiritite—silicified serpentinite consisting mostly of quartz with only minor carbonate and relict Cr-spinel (Akbulut et al., 2006; Lacinska & Styles, 2013; Nasir et al., 2007; Stanger, 1985)—or magnesite-fuchsite rocks that contain only traces of quartz (Menzel et al., 2018). Thermodynamic models suggest that both birbiritites and magnesite-rich rocks can be the result of extended fluid-rock interaction to high water/rock ratios after listvenite formation at different temperatures (Klein & Garrido, 2011).

A very interesting and not well-understood aspect of the hydration and carbonation of peridotite is how these reactions can go to completion. Because solid mass is increased by addition of H₂O and CO₂, and the hydrated and carbonated solid products have lower densities than the solid reactants, reactions increase the solid volume. Fluid-rock reactions that increase the solid volume may clog porosity, reduce permeability, and produce reaction rims that passivate the reactants (Andreani et al., 2009; Farough et al., 2016; Godard et al., 2013; Oelkers et al., 2018; van Noort et al., 2017). Accordingly, observations in experiments of carbonation of natural peridotite by several groups (Andreani et al., 2009; Godard et al., 2013; Hövelmann et al., 2013; van Noort et al., 2017) showed decreasing permeability, suggesting that the carbonation reaction was self-limiting in these experiments. However, in nature, replacement of peridotite by carbonates can proceed to completion, as shown by listvenites. A key to how this process goes to completion may be hierarchical fracture networks, where the crystallization pressure creates local gradients in differential stress and drives fractures, which in turn increase permeability and reactive surface area (e.g., Malthe-Sørenssen et al., 2006; O'Hanley, 1992; Rudge et al., 2010; Ulven et al., 2014), as experimentally demonstrated for hydration of periclase (Zheng et al., 2018). On a larger scale, volume change may also cause differential stress and fracture, as proposed for olivine hydration by Macdonald and Fyfe (1985). Alternatively, anisotropic far field stress in tectonic deformation can lead to dilatancy and allow the reaction to go to completion.

A review by Kelemen and Hirth (2012) suggests that the crystallization pressure during carbonation of peridotite can be very large, and argues that this process can lead to a positive feedback due to cracking, allowing the reaction to go to completion. Phase field models suggest a positive feedback between reaction-driven cracking and the local rate of peridotite hydration in hierarchical vein networks (Evans et al., 2020), a process that may also apply to carbonation reactions. Zhu et al. (2016) conducted a mineral carbonation experiment on olivine using synchrotron X-ray microtomography, which showed polygonal cracks propagating into the interior of the olivine aggregate. They infer that nonuniform volume expansion induced by the reactions generates polygonal cracking of the surfaces. In addition, the reaction products may be microporous to nanoporous, providing fluid pathways through the matrix, which may cause microstructural maintenance and enhancement of permeability via combined dissolution and precipitation processes (Malvoisin et al., 2020; Peuble et al., 2015; Tutolo et al., 2016). Studies propose that dissolution etch pits along dislocations in olivine are preferentially filled with reaction products and form the nucleus for microcracks (Klein et al., 2015; Peuble et al., 2018; Plümper et al., 2012; Xing et al., 2018).

Brittle deformation may therefore play a key role in increasing the reactive surface area and maintaining or enhancing permeability. Accordingly, some engineering approaches to carbon sequestration by olivine carbonation achieve higher reaction rates by powdering of the reactant material (e.g., Li & Hitch, 2018, and references therein). However, in the absence of continued deformation during reaction, permeability reduction and passivating silica reaction rims often prevail and inhibit complete carbonation (van Noort et al., 2017). Compaction and triaxial deformation experiments suggest mechanically enhanced dissolution rates during hydration and carbonation of olivine (Lisabeth et al., 2017). In natural reservoir and crustal conditions, mechanically enhanced reaction rates are likely to occur in brittle fault zones that are characterized by high permeability and renewal of reactive surfaces due to faulting and cataclasis. Listvenites are indeed often related to major thrust faults and show evidence of brittle deformation such as tectonic breccias and veins (Escayola et al., 2009; Hansen et al., 2005; Menzel et al., 2018; Qiu & Zhu, 2018).

The Samail ophiolite in Oman includes large surface exposures of variably hydrated and carbonated mantle rocks—an ideal place to study the interaction between rock deformation and peridotite alteration.

Listvenites occur along the basal thrust of the ophiolite in the Samail massif (Nasir et al., 2007; Wilde et al., 2002). Previous field, geochemical, and microstructural studies of the Oman listvenites (Falk & Kelemen, 2015; Kelemen et al., 2011; Nasir et al., 2007; Rajendran et al., 2013; Stanger, 1985) did not address how the transformation of peridotite to listvenite could proceed at a large scale. In parts this is due to the outcrop conditions with thick weathering crusts and abundant fracturing, which also hindered a systematic study of deformation structures. Hole BT1B of the Oman Drilling Project was drilled for this reason, to acquire a fresh core from a continuous section from listvenite into the metamorphic sole that would allow systematic (micro)structural and geochemical logging of the carbonation reaction processes. The tabular nature of listvenite bands in partially serpentinized peridotite at Oman Drilling Site BT1, parallel to the gently dipping basal fault of the ophiolite, suggests that large-scale, imbricate faults may have played a role in guiding the CO₂-bearing fluids that formed listvenite.

Here we present evidence of multistage brittle deformation in listvenites and serpentinites based on field observations, visual core inspection, and petrography, using the unique sample set from Hole BT1B. The aim of this contribution is to study whether widespread cataclasites in the Oman listvenites are coeval with carbonation and are examples of mechanically enhanced reaction rates or whether they postdate listvenite formation. In order to evaluate the possibility of postobduction tectonic overprint for cataclasite formation in listvenite, we further compare the cataclasite and fault microstructures and conditions with postemplacement structures in the underlying carbonate-bearing units.

2. Geological Setting

2.1. Tectonic Evolution of the Oman Mountains

The Samail ophiolite (Figure 1a) exposes a relatively intact sequence of obducted oceanic crust (4–8 km thick; Nicolas et al., 1996) and mantle (9–12 km thick in the Wadi Tayin massif; Hanghøj et al., 2010; Hopson et al., 1981) formed during the Cenomanian (96.5–95.5 Ma; Rioux et al. (2013)) at a fast-spreading mid-ocean ridge or a suprasubduction zone spreading center (Coleman, 1981; Glennie et al., 1974; Searle & Cox, 1999). Intraoceanic subduction of oceanic crust and sediment slices led to the formation of a high-grade metamorphic sole beginning at about the same time as ophiolite formation (Hacker et al., 1996; Rioux et al., 2013) or up to 10 Ma earlier (Guilmette et al., 2018; Soret et al., 2020). The sole records amphibolite to granulite facies peak metamorphic conditions (530–850°C, 0.5–1.0 GPa) and was exhumed along with peridotite at the basal thrust during ophiolite obduction (Cowan et al., 2014; Ghent & Stout, 1981; Hacker & Mosenfelder, 1996; Soret et al., 2017). The emplacement of the Samail ophiolite occurred by obduction onto allochthonous distal sediments (the Hawasina formation) in the first, intraoceanic subduction stage, and subsequent top-to-S thrusting of both ophiolitic and allochthonous sediment nappes onto the thick autochthonous sediments of the Mesozoic passive margin of the Arabian plate (e.g., Searle & Cox, 1999). The Jebel Akhdar and Saih Hatat anticlinoria, exposed in peaks up to 3,000 m high in the Al Hajar mountain range, form large-scale tectonic windows that permit the reconstruction of postobduction tectonics that affected the continental carbonate platform due to the emplacement of the Hawasina and ophiolite nappes (Figure 1a). Partial subduction and burial of the passive margin below the ophiolite nappe caused heating to different peak metamorphic conditions from 450–550°C, 2.0–2.4 GPa, in eclogite of the deepest As Sifah complex NE of the Saih Hatat dome, to 280–360°C, <0.5–1.0 GPa, in the NW Saih Hatat (Agard et al., 2010; Miller et al., 1999; Saddiqi et al., 2006; Searle et al., 1994), and 300–360°C, 0.28–0.34 GPa (lithostatic pressure), recorded in veins in carbonates of the Jebel Akhdar dome (Grobe et al., 2019). The burial caused fluid overpressure, and generation and migration of hydrocarbons, but little deformation in the carbonate platform (Grobe et al., 2016). This was followed by top-to-NNE ductile shear zones (Al-Wardi & Butler, 2007; Grobe et al., 2016), the deformation of earlier veins, and the formation of mylonitic marbles in the early Campanian (~80–60 Ma) (Grobe et al., 2018). Normal and oblique-slip faults with horst-graben structures formed during Campanian to Maastrichtian times, after ophiolite obduction, with extension and dome exhumation (Grobe et al., 2018) accompanied by subaerial erosion of the ophiolite followed by deposition of shallow marine carbonates (e.g., Nolan et al., 1990). This was followed by NE-SW shortening in the Miocene to Pliocene during large-scale folding of the Jebel Akhdar and Saih Hatat domes, which tilted the earlier structures (Gomez-Rivas et al., 2014; Grobe et al., 2018). Widespread strike-slip faults postdate the large-scale folding (Gomez-Rivas et al., 2014; Grobe et al., 2018; Virgo et al., 2013). At the

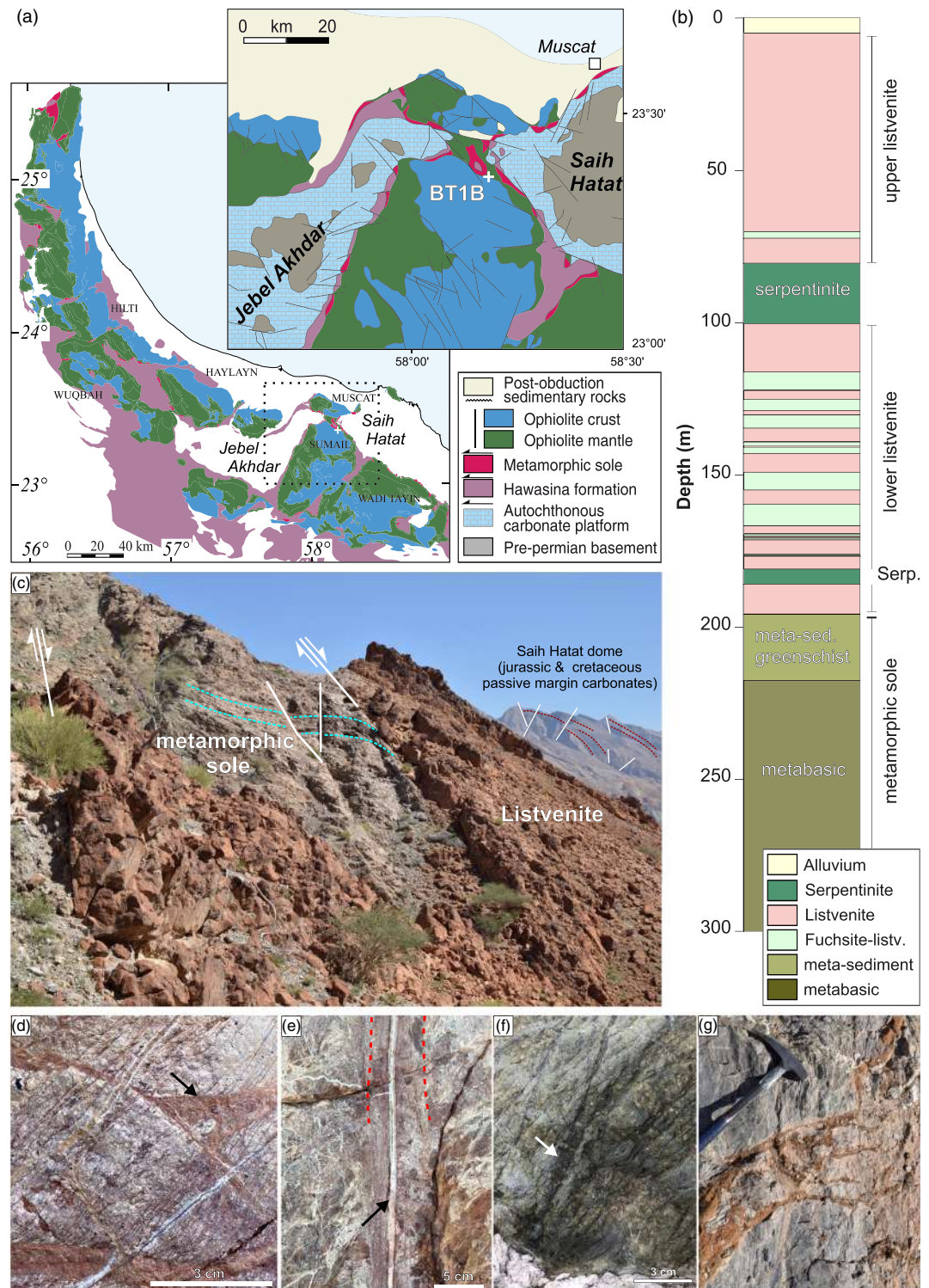


Figure 1. (a) Simplified geological overview map of Northern Oman (after Nicolas & Boudier, 1995) and geology of the northern Samail massif (after Béchenec et al., 1992); (b) lithological column of Hole BT1B; (c) field view of the contact between listvenite and greenschists of the metamorphic sole looking east, with the Saih Hatat dome in the background; (d) red-stained cataclasite in listvenite, cut by white-yellowish dolomite veins; (e) listvenite cataclasite (marked red) reactivated by a sharp fault with quartz/carbonate vein (arrow); (f) black cataclasite in serpentinite; and (g) red oxidized cataclasite in metasediments of the metamorphic sole.

northern flank of Jebel Akhdar, final exhumation of the core of the anticlinorium occurred along detachments (Grobe et al., 2018).

Fluid inclusion thermobarometry of veins related to faulting in the Jebel Akhdar and Saih Hatat domes indicates that much of the tectonic evolution occurred under the overburden of the ophiolite (Grobe et al., 2019). Hence, the tectonic events observed in the carbonate platform probably affected the ophiolite as well, although this has not been studied in detail.

2.2. Listvenites in the Samail Massif and Hole BT1B

Listvenites are common in the northern part of the Samail massif of the Samail ophiolite, Oman, where they form red- to orange-colored ridges that have a higher resistance to weathering than peridotite. Historically, these listvenites were also called the Amqat unit (Glennie et al., 1974; Stanger, 1985). The listvenites occur along the basal thrust of the ophiolite where peridotite is in contact to the metamorphic sole (Nasir et al., 2007). The largest outcrops are in lenses along the transition from the Jebel Akhdar to the Saih Hatat domes of the Al Hajar mountain range (Falk & Kelemen, 2015; Stanger, 1985; Villey et al., 1986; Wilde et al., 2002). Minor listvenite bodies also form tectonic blocks in shear zones within Hawasina metasediments and the metamorphic sole of the same area (Nasir et al., 2007).

The listvenites at Wadi Mansah are an outstanding natural example showing that peridotite carbonation reactions can go to completion on large scale (Falk & Kelemen, 2015). Where listvenite is in contact with serpentinized peridotite, the presence of intergrown antigorite + quartz \pm talc suggests temperatures of 80–130°C, broadly consistent with clumped-isotope thermometry of carbonates (45–245°C; Beinlich, Plümper, et al., 2020; Falk & Kelemen, 2015), and the presence of microcrystalline quartz (recrystallized from opal or chalcedony) (Streit et al., 2012). An internal Rb-Sr isochron gives an age of 97 ± 29 Ma (Falk & Kelemen, 2015), in agreement with the age of emplacement of the ophiolite. Age corrected to 96 Ma, $^{87}\text{Sr}/^{86}\text{Sr}$ values in the listvenite are consistent with those of the underlying Hawasina metasediments (Falk & Kelemen, 2015).

Hole BT1B of the Oman Drilling Project (International Continental Drilling Project Expedition 5057-4B) was drilled in Wadi Mansah (lat. 23.3643°; lon. 58.1827°) in March 2017, to sample a continuous, unweathered section of listvenite, serpentinite, and the metamorphic sole (Figure 1a). The BT1B core has 100% recovery and includes about 200 m of listvenite intercalated with serpentinite (Figure 1b). An upper section of 70 m of listvenite is followed by 20 m of carbonate-bearing serpentinite. A lower 80 m section of listvenite includes several domains rich in chromian mica (light green layers in Figure 1b) and is underlain by 5 m of serpentinite. All of the listvenite-serpentinite contacts are intact and gradational and usually marked by domains of ophicarbonates. The lowermost 10 m of listvenite is separated from the metamorphic sole by 10 cm of black cataclasite and clay fault gouge, which forms part of the basal fault of the Samail ophiolite. Below the listvenites and fault gouge, the BT1B core contains 100 m of the metamorphic sole, comprising 20 m of metasedimentary rocks and ~80 m fine-grained metamafic rocks (Figure 1b).

While many calcite- and dolomite-bearing listvenites and birbirites (silicified serpentinite) in the northern Samail massif have highly variable Mg/Si ratios and Ca contents (Falk & Kelemen, 2015; Nasir et al., 2007; Stanger, 1985), the conversion of peridotite to magnesite-rich listvenite at the site of Hole BT1B was nearly isochemical on the whole-core scale except for the addition of CO₂. Average bulk rock Mg/Si, Fe/Si, Al/Si, Fe/Mg, and Cr/Al ratios in listvenite are similar to the average composition of the Samail peridotite, while CaO and correlated Sr are higher, most likely derived from underlying sediment (Falk & Kelemen, 2015; Godard et al., 2017; Kelemen et al., 2017, 2020). Thus Mg, Si, Al, and Cr, plus Fe were largely immobile on a ~10 m scale during introduction of C, O, lesser Ca, minor Fe, and mobile trace elements during transformation of Mg-silicates to carbonate + quartz (Kelemen et al., 2020). This implies a large solid volume expansion of >50% compared to partially serpentinized Oman peridotite (Kelemen et al., 2020) or 18–21% relative to a serpentinite protolith. Fe-oxides traces in listvenite that resemble the typical mesh microstructure of olivine serpentinization suggest that some (if not all) of listvenite in BT1B has formed from a serpentinite protolith (Beinlich, Plümper, et al., 2020; Kelemen et al., 2020; Lafay et al., 2020). Hence, the required solid volume increase may have occurred in a two-step process related to initial serpentinization followed by listvenite formation.

3. Methods and Materials

3.1. Visual Core Logging

Cores of Hole BT1B were logged onboard R/V Chikyu in September 2017 by the Oman drilling Phase 1 science team following IODP logging standards (Kelemen et al., 2020). During the macroscopic core logging the host rock was characterized as massive, brecciated, foliated, sheared, cataclastic, or fragmented by veins if the host rock structure was completely obscured by a high vein density. For planar structures that crosscut the host rock, orientation and width could be determined; of these, individual veins, sets of veins, cataclases, (semi)ductile shear zones, and sharp faults were distinguished. Cataclases were identified based on the observation of clast sliding and rotation, and fragmentation of particles into a fine-grained matrix (Passchier & Trouw, 2005). First results and data sets of the onboard core logging are available in the corresponding chapter of the IODP/ICDP Proceedings of the Oman Drilling Project (Kelemen et al., 2020). For this study, we revisited cataclastic structures identified in the onboard logs by inspecting split core images in detail in order to improve the consistency of the data set with regard to these brittle structures. For clarity, we do not distinguish in the following between host rock and localized structures, or between cataclase and tectonic breccia (as done in Kelemen et al., 2020), but use the term cataclase for all intervals of brittle deformation that meet the criteria of clast sliding, rotation, and substantial fragmentation into highly variable clast sizes (Passchier & Trouw, 2005).

3.2. Samples

Samples were selected during onboard drill core logging following different criteria, covering the broad (micro)structural and textural diversity of the listvenites to identify the structures related to different stages of carbonation reaction process as opposed to overprinting structures after listvenite formation. For this study, we inspected thin sections from 105 samples for the presence of cataclases. Thin sections from 27 samples that contain cataclases have been selected for detailed study (supporting information Table S1).

3.3. Virtual Polarizing Microscopy (ViP)

A high-resolution virtual polarizing microscope platform (ViP) recently developed by the Institute of Structural Geology, Tectonics and Geomechanics (GED, RWTH Aachen University) and the Fraunhofer Institute for Life Science Informatics (Virgo et al., 2016) was used for microstructural analysis.

The thin sections selected for this study were scanned in plane-polarized and reflected light, and with crossed polarizers at 10 different polarization angles, using a 10× objective. The image data were then processed to extract the extinction curve of each “super pixel,” producing gigapixel images of the extinction behavior at all polarization angles, which allows for multiscale image analysis. Virtual polarizing microscopy data sets are publicly available via the Oman Drilling Project data repository of the ICDP, together with a virtual microscopy software (TileViewer) that is user friendly and allows Google Earth—like zooming and browsing through the thin section as well as rotation of the polarizers and switching between illumination conditions (<https://www.icdp-online.org/projects/world/asia/oman/details/>).

3.4. Electron Microscopy (SEM-EDS)

A Zeiss Gemini SUPRA 55 field-emission electron microscope at the Institute of Structural Geology, Tectonics and Geomechanics (RWTH Aachen University) was used for phase identification and automated energy-dispersive X-ray spectroscopy (EDS) mapping of thin sections. Samples were coated by a 6–8 nm thick layer of tungsten for conductivity. Operating conditions were 3 kV and ~5 mm working distance for high magnification imaging, and 15 kV and 8.5 mm working distance for EDS analysis, at high vacuum, respectively. A dwell time of 200 μs/point was chosen for EDS mapping of whole thin sections.

3.5. Image Analysis and Grain Size Distributions

The EDS data and backscattered images were processed by applying noise reduction filters and defining thresholds in ImageJ to produce phase maps for the major minerals. Distinction between quartz and amorphous silica, or between magnetite, hematite, and Fe hydroxides, was not possible for large area EDS mapping. We used the particle analysis tool of ImageJ to determine the grain size distribution in selected representative areas of cataclase, following an approach similar to that of Keulen et al. (2008). Due to the phase variability and the matrix cementation by silica and Fe (hydr)oxides in many cataclases, particles were segmented based on magnesite phase maps from EDS data and on plain polarized ViP microscopy

scans. SEM-EDS data allow for higher resolution, whereas the gigapixel ViP microscopy images provide the particle size distribution of both mineral and lithic clasts on the whole thin-section scale while filtering out the parts of the cataclasite affected by Fe-(hydr)oxide staining and cementation. Late carbonate veins cross-cutting the cataclasites have been filtered out based on the particle aspect ratio. To measure the grain size distributions of clasts, the relative frequency of grain areas normalized to the image area and the bin width have been calculated as the number of grains N_i in each bin i , using five logarithmic spaced bins per order of magnitude. Plotting the relative frequency against the grain area in log-log plots yields the local linear slope D of a possible power law distribution (Keulen et al., 2008; Laurich et al., 2018).

4. Results

4.1. Field Relations

Listvenites in the Wadi Mansah and Fanjah regions of the Samail massif form meter to decameter thick bands within serpentinite and along contacts between serpentinite and the metamorphic sole (e.g., Figure 1c). Commonly two or three such listvenite bands are intercalated in serpentinite and can be followed for several kilometers along strike. Contacts between listvenite and variably serpentinitized peridotite are either gradational—composed of a 0.5–3 m wide transitional zone of carbonate-bearing serpentinite—or consist of strongly deformed, up to 3 m wide serpentinite fault gouge. Partially hydrated, layered peridotite (i.e., dunite-harzburgite with low degree of serpentinitization) was not found in direct contact with listvenite; instead they are separated by a 3–20 m wide layer of (carbonate-bearing) serpentinite, locally with intergrown serpentine and quartz, and/or mineral assemblages including talc (Falk & Kelemen, 2015; Manning et al., 2017). Contacts between listvenite and greenschist-to-amphibolite facies rocks of the metamorphic sole, Hawasina metasediments, layered gabbro, and Tertiary sediments are commonly characterized by faults with abundant cataclasites and locally 0.3 to >5 m of serpentinite fault gouge. Broad folding of the basal fault of the ophiolite north of Wadi Mansah may have locally inverted the original shear sense of these faults. At the southern fold limb, drag folds and striae on slip surfaces at the contacts to the metamorphic sole indicate an apparent top-down sense of shear (Figure 1c).

Faults and cataclasites (<5 mm to 2 m wide) are common in the listvenites in the Samail massif (e.g., Figures 1d and 1e). Striae on fault planes in listvenite suggest an apparent normal, oblique normal, or strike-slip sense of shear. Locally, nearly vertical strike-slip faults cut the faults that form the contact between listvenite and the metamorphic sole, with offsets of several meters, indicating that faulting along the contact occurred during an earlier phase of deformation. In general, tilting and rotation of large fault blocks, folding, and the lack of clearly defined marker horizons make it difficult to reconstruct the true sense of shear for the faults in listvenites and serpentinites. Cataclasites in listvenites are cohesive, and their sense of shear is often not possible to determine in outcrops. Lithic listvenite clasts in cataclasite are slightly rounded to angular and up to 5–10 cm in diameter. The cataclasites are cemented by a matrix that is often stained red (silica-rich cataclasites with Fe oxides) or yellow (dolomite-rich cataclasites) in outcrops. In the field, cataclasites are also widespread along fault zones within schist of the metamorphic sole, where they crosscut the metamorphic foliation (Figure 1g), and in late Paleocene conglomerates that unconformably overlie the ophiolite NE of the village of Fanjah. In serpentinite, it is difficult to detect clear and cohesive cataclasites due to weathering, but occasionally, black (ultra)cataclasites are discernible (Figure 1f).

4.2. Hole BT1B

Core logging has revealed a diverse petrology and structure, from serpentinite with peridotite relics, massive listvenite, foliated listvenite, several generations of veins, ductile shear zones, cataclasite, breccia, and planar faults (Kelemen et al., 2020). The density of veins in the core is very high, >100 per m (Manning et al., 2017). Both the serpentinite and listvenite contain and are overprinted by several generations of veins, cataclasites, sharp planar faults, and late, partially open veins. The earliest type of magnesite vein, which occurs in both serpentinite and listvenite, is antitaxial. In the upper part of Hole BT1B, this earliest vein type includes a median line rich in iron oxides (hematite and goethite). Quartz + chalcedony ± carbonate veins are syntaxial and younger, based on crosscutting relationships. These structures are overprinted by cataclasites and breccia, often enriched in iron oxides, and sharp, planar faults with silica or carbonate veins on the slip surface. Syntaxial, partially open veins of magnesite or dolomite are the latest structures. Crosscutting relations may

not be the same everywhere in the core, and structures belonging to one generation may or may not be synchronous.

Listvenite not affected by overprinting (i.e., “primary listvenite”) can be massive, containing spheroidal magnesite grains and pseudomorphs of the typical mesh and bastite textures of serpentinite (Beinlich, Plümper, et al., 2020; Jöns & Bach, 2013; Kelemen et al., 2020; Lafay et al., 2020). In other parts of the core, primary listvenite has a well-developed foliation defined by lithological banding and at the microscale ellipsoidal carbonate particles with an iron oxide core. Shear bands with a locally well-developed foliation are common in the serpentinite, and also in the transition between serpentinite and listvenite, where there are no discernible faults or cataclasites (Kelemen et al., 2020).

In the lower 100 m of Hole BT1B, greenschist-to-epidote amphibolite facies phyllitic-to-schistose metasediments and foliated metabasic rocks are characterized by early ductile shear fabrics with tight isoclinal folds, likely related to subduction and/or exhumation (Kelemen et al., 2020; Kotowski et al., 2020). These earliest ductile fabrics are crosscut by epidote-quartz veins, shear zones, thrust-sense chloritized microfaults, minor breccias and cataclasites, and late, normal-sense carbonate-filled microfaults (Kotowski et al., 2020). Cataclasites and breccias in the metamorphic sole potentially correlate with those in listvenite, but because the timing of tectonic juxtaposition of the listvenites and serpentinites with the metamorphic sole and its role for listvenite formation remain unclear (Kotowski et al., 2020), we focus in the following on cataclastic listvenites.

4.2.1. Macroscopically Identified Cataclasites in Hole BT1B

Figure 2 shows a plot of the occurrences of macroscopically identified cataclasites with depth, the downhole log of magnetic susceptibility and shipboard porosity measurements, and split core images of cataclasites in listvenite and serpentinite in the upper 200 m of Hole BT1B. Cataclasites occur throughout most of the core, with particularly thick or abundant cataclasite intervals between 5–18, 51–55, 146–151, 166–172, and 185–192 m depth (Figures 2a and 2b). A 55 cm wide fault gouge (Figure 2l) forms the contact between listvenite and the metamorphic sole at 197 m depth. This clay-rich, granular gouge is texturally distinct from the cohesive cataclasites within listvenite core.

In total 352 cataclasites were identified macroscopically in the upper 200 m of Hole BT1B, with a cumulative width of about 21 m (Figure 2b). Hence, about 10 vol% of listvenite and serpentinite in Hole BT1B is composed of cataclasite. This estimate only includes sections where clast rotation and a high degree of fragmentation typical of cataclasis occurred; the additional thickness of damage zones with cracked grains and a high abundance of small-scale faults in the rock adjacent to cataclasites is often substantial.

The width of single cataclasite bands varies significantly throughout the core (0.1 cm to 1 m). For wide cataclasites, orientation and true thickness could not be determined from the core sections and the estimated true width is somewhat uncertain. The lack of macroscopically visible cataclasites does not exclude their presence: In several cases, <1 mm wide cataclasite bands are visible in thin sections of samples without macroscopically visible cataclasis. Most listvenite cataclasites are cohesive, featuring similar bulk rock porosities as listvenite (red and blue data points in Figure 2c), and form anastomosing and branched bands (Figures 2f and 2g). Wide cataclasites (>3 cm) occasionally display internal flow banding of small-grained matrix-rich domains that envelop coarse, variably cracked clasts (Figures 2e and 2k). Locally several cataclasite generations overprint each other and are crosscut by sharp faults (e.g., Figure 2e). Fe-hydroxide staining is common in the matrix of many cataclasites, in particular in the upper 60 m of Hole BT1B. Some of these red-stained cataclasites correspond to comparatively low magnetic susceptibilities as measured by multisensor core logging of whole-round core (Kelemen et al., 2020), representing strongly oxidized intervals; but there is no clear correlation since low magnetic susceptibilities also occur in intervals without cataclasites (Figure 2c). Cataclasites in the serpentinite layers typically have gray to green color, consisting of serpentinite clasts with a carbonate-rich matrix (Figure 2i); only rarely they are stained red by Fe hydroxides (Figure 2h). Hence, serpentinite cataclasites are not particularly oxidized relative to serpentinite but likely contain magnetite, showing no or minor excursions to comparatively lower magnetic susceptibility (Figure 2c).

The amount of displacement related to cataclasites is rarely measurable in the core (e.g., Figure 2f), perhaps because many have displacements larger than the 6.4 cm (HQ) and 4.8 cm (NQ) core diameter. However, there are no cataclasites containing listvenite or metamorphic sole lithologies within serpentinite host

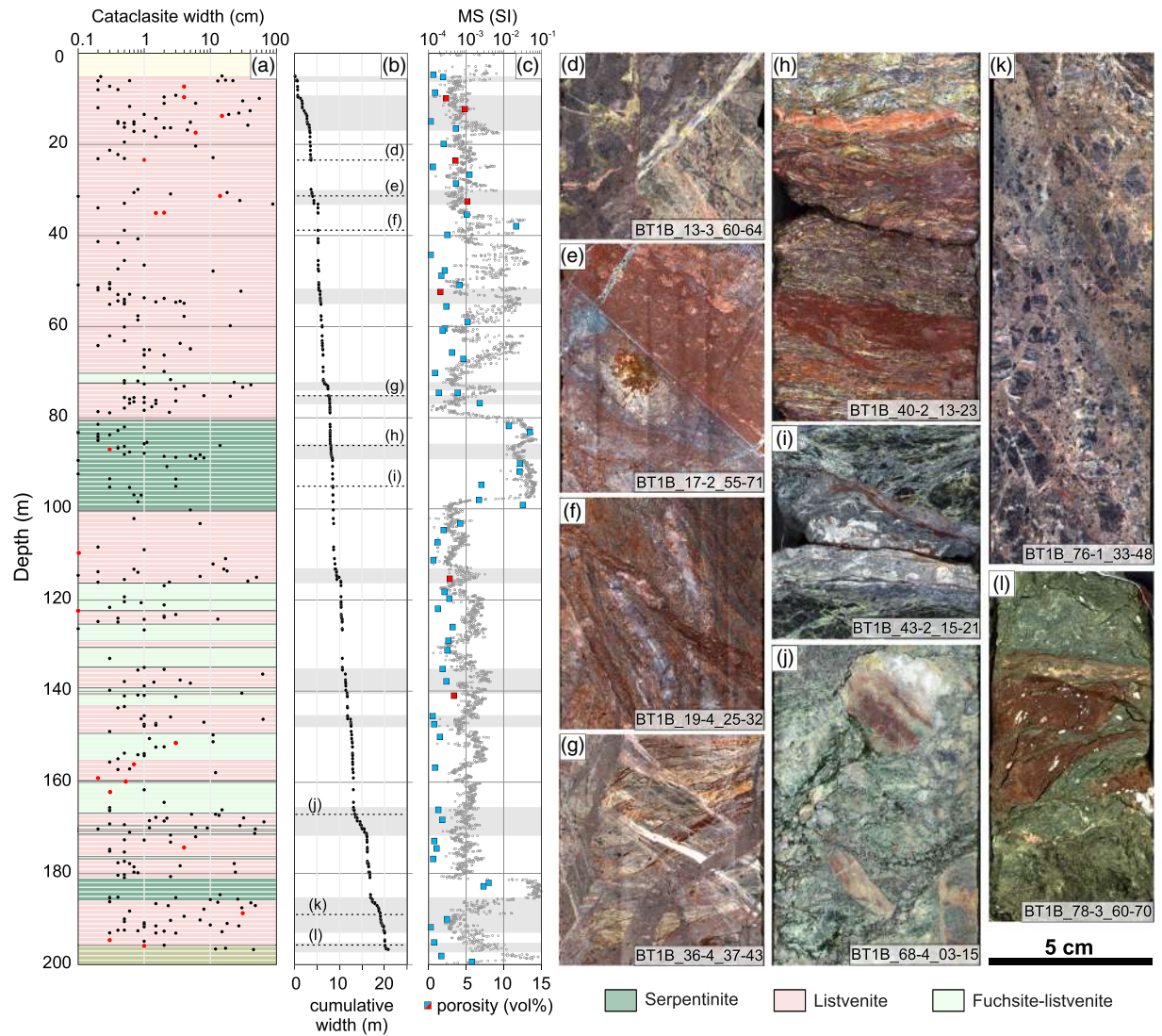


Figure 2. Macroscopically identified cataclasites in the upper 200 m of Hole BT1B. Downhole plots of (a) occurrences and apparent width of all logged cataclasites (red data points show cataclasites confirmed in thin section; color coding of lithologies is the same as in Figure 1b); (b) the cumulative width of cataclasites with depth; and (c) magnetic susceptibility (MS) from multisensor core logging and porosity from discrete shipboard measurements in the upper 200 m of Hole BT1B (data from Kelemen et al., 2020; red porosity data points are from samples that contain or are close to cataclastic listvenite). Gray shadings in (b) and (c) highlight intervals with abundant or major cataclastic bands. Further shown are split core images of examples of (d–g) cataclasites in the upper listvenites, (h, i) cataclasite in the upper serpentinite layer, (j, k) cataclasite in the lower listvenites, and (l) fault gouge at the contact to the metamorphic sole. The corresponding depth of these examples in Hole BT1B is indicated in (b).

rocks, none containing serpentinite or sole lithologies within listvenite, and none containing listvenite or serpentinite within the sole, suggesting that displacements along the cataclasites near contacts are less than a few meters.

4.2.2. Microstructure of Cataclasites in Listvenites

Cataclasites are composed of quartz/chalcedony, magnesite, dolomite and oxide mineral clasts (grain sizes ranging from below 0.2 to 500 μm), and different lithic clasts of variable size. Magnesite mineral clasts are very common in cataclasite, whereas larger quartz clasts are rare (probably due to the generally small grain size of quartz/chalcedony in the host listvenite). Lithic clasts can contain fragments of listvenite composed of magnesite spheroids and interstitial quartz—a common microstructure in listvenite of Hole BT1B (Figure 3). Larger clasts occasionally contain fragments of veins that crosscut the listvenite. Other lithic clasts are fragments of magnesite veins, chalcedony-magnesite veins, quartz veins, breccia, and cataclasite. Clasts are commonly rotated and rounded—in particular where cataclasites have been reactivated several times

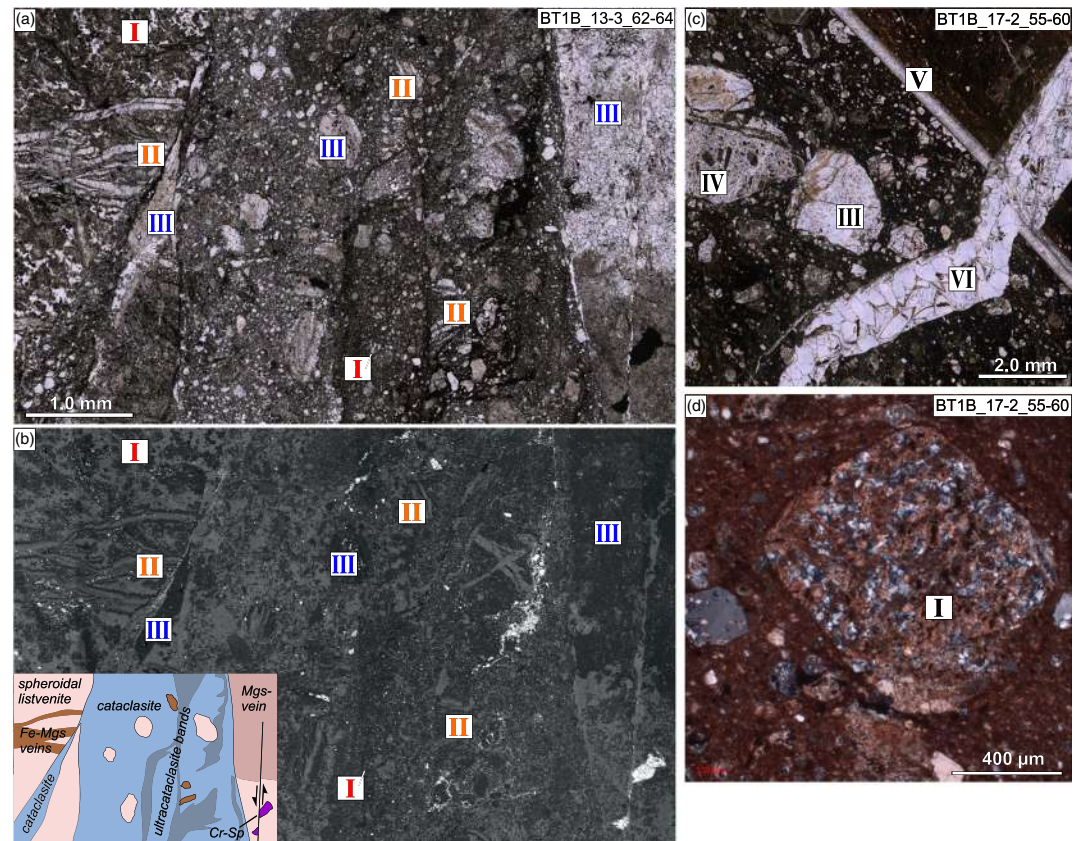


Figure 3. Listvenite cataclasite microstructures. (a, b) ViP plane-polarized (ppol) micrograph and BSE image of localized cataclasite, showing clasts of listvenite with magnesite spheroids (I) and vein fragments (II, III), and corresponding microstructures in the host listvenite. A simplified interpretative sketch is given in the inset in (b). (c) Reworked cataclasite with breccia clast (IV). A sharp fault with dolomite-calcite and quartz veins (V), and a dolomite vein (VI) crosscut cataclasite (ViP ppol). (d) Clast with magnesite spheroids and Fe-hydroxide staining in cataclasite matrix (crossed polarizers).

(Figure 3c). Magnesite mineral clasts locally show a chemical zonation of Fe contents—similar to magnesite in host listvenite (e.g., Beinlich, Plümper, et al., 2020; Lafay et al., 2020). The Fe zonation is truncated sharply at the rims of magnesite clasts (Figure 4b). Relict Cr-spinel is strongly fragmented (grain sizes 0.5 to 500 μm) and can serve as a strain indicator where stretched into trails of dismembered grains (Figure 4a). Red staining of some cataclasites is due to fine-grained hematite and goethite (<20 μm) that decorate clast rims and occur interstitially in the fine-grained matrix. In contrast to angular and fragmented Cr-spinel, hematite in the cataclasite matrix displays subhedral to euhedral grains that are partly rounded or form small acicular and atoll-shaped aggregates (Figure 4b). The smallest grain size fraction (matrix) is commonly dominated by quartz/chalcedony and a smaller proportion of magnesite fragments. Dark-colored, discontinuous ultracataclasite seams and bands (<100 μm wide) occur within cataclasites and at their boundary with the listvenite host rock, commonly oriented subparallel to the main cataclasite. Sharp faults often crosscut cataclasites or are localized along their contact with the host listvenite.

Clast sizes from 50–50,000 μm^2 in a prominent cataclasite at 31.4 m depth (Sample BT1B_17-2_55-60) follow a power law distribution with D values of ~ 1.9 – 2.0 (Figure 5). Such D values are typical for cataclasites and fault gouges that are characterized by extensive clast rotation and displacement (e.g., Billi, 2007; Keulen et al., 2008; Laurich et al., 2018). Cataclasites that overprint preexisting cataclasite contain fewer large clasts and a higher matrix fraction.

4.2.3. Crosscutting Relationships

With the exception of the youngest generation of carbonate veins (usually dolomite or dolomite-calcite), most other microstructures in host listvenite are truncated by cataclasites, and fragmented clasts of these earlier structures are present within the cataclasites. The microstructures overprinted by cataclasite

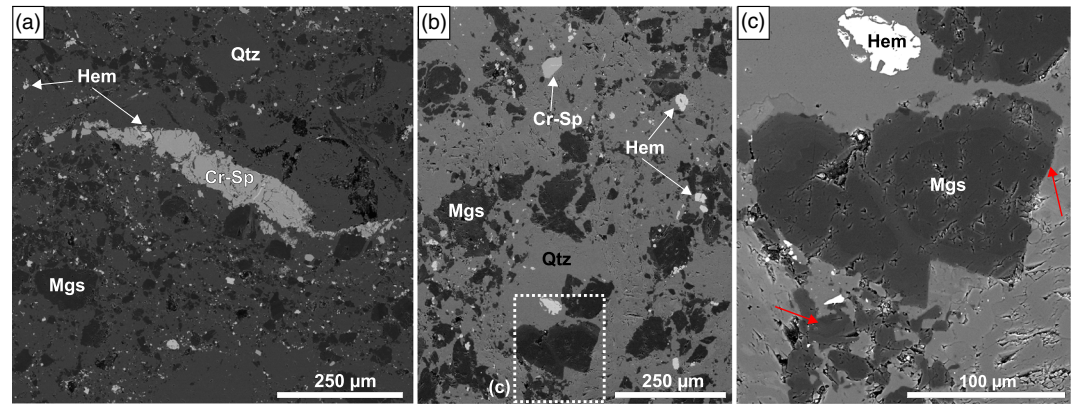


Figure 4. BSE images of Fe (hydr)oxide-stained cataclasites. (a) Stretched and fragmented Cr-spinel suggesting sinistral shear (Sample BT1B_17-2_55-60). (b) Angular fragments of Cr-spinel versus rounded to subhedral hematite grains and aggregates in cataclasite matrix. (c) Detail from (b), showing truncation and fragmentation of chemically zoned magnesite clast (red arrows). (b, c) Sample BT1B_9-3_28-31; in these images contrast and brightness have been adjusted to enhance visibility of the zonation in magnesite.

include host listvenite with a spheroidal to euhedral magnesite habit (Figures 3a, I, and 3d), foliated listvenite (Table S1, Sample BT1B_78-2_34-38), antitaxial magnesite veins displaying Fe zonation (Figure 3a, II), microcrystalline quartz veins, and magnesite-chalcedony veins (Figure 3a, III). Besides truncation and fragmentation of host listvenite structures, different cataclasite generations overprint each other, with thin localized cataclasite bands crosscutting or reactivating older ones (cf. breccia clast in cataclasite, Figure 3c, IV).

Figure 6 is a good example of the youngest microstructures and their crosscutting relations in Hole BT1B, showing a sharp fault juxtaposing two distinct cataclasite generations (α and β in Figure 6). The highly localized slip plane is marked by an up to 1.5 mm wide, red-stained ultracataclasite band (γ , Figure 6) and by a 250 μm wide vein of microcrystalline quartz precipitated after faulting. Cataclasites, fault, and the quartz vein were then crosscut by syntaxial, coarse-grained dolomite veins.

The youngest microstructure is a dolomite-calcite vein that partly follows the quartz vein along the fault plane and deflects into the dolomite vein. This is consistent with the observation that the youngest veins in field outcrops and throughout Hole BT1B often are composed of dolomite (\pm calcite), forming syntaxial veins, partially open veins, and the matrix of hydraulic/hydrothermal breccias.

4.2.4. Chemical Characteristics of Cataclasite

SEM-EDS chemical mapping shows that in many cases, fluid flow during or after cataclasis modified the Mg/Si ratio of listvenite affected by brittle deformation. Different cataclasite generations that overprint each other are affected to variable extent by this chemical modification. Reconstructed EDS spectra of two $\sim 400 \text{ mm}^2$ areas of different cataclasite generations juxtaposed by a fault in a large thin section of Sample BT1B_17-2_55-60 reveal that gray-red cataclasite with a more abundant coarse clast fraction has a molar Mg/Si ratio of ~ 0.49 (α in Figure 6). This is significantly lower than the average molar Mg/Si of harzburgite (1.52–1.54) and dunite (1.75–1.80) of the Samail ophiolite (Godard et al., 2000; Hanghøj et al., 2010; Monnier et al., 2006) and lower than average listvenite in Hole BT1B (~ 1.48 ; Kelemen et al., 2020). Red-stained, finer-grained cataclasite in the area above the fault shows more rounded mineral and lithic clasts and has even lower Mg/Si of ~ 0.18 (β in Figure 6). And the Mg/Si ratio is as low as 0.01 in the 1.5 mm wide, silica-dominated ultracataclasite band adjacent to the fault slip plane, which is mostly composed of a fine-grained matrix with only few clasts

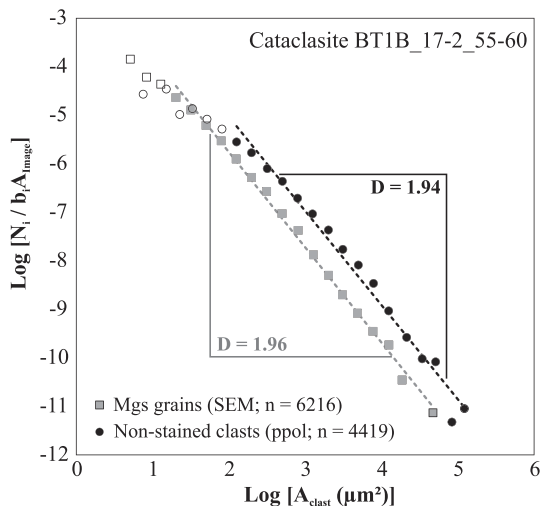


Figure 5. Grain size distribution of listvenite cataclasite, showing a log-log plot of clast frequency N_i versus area A . Frequency is normalized to the bin width and the image area, for five logarithmic bins per order of magnitude. Similar D values (slope of the power law fit to curves) are obtained from image segmentation of magnesite grains (by SEM-EDS mapping) and from clasts that are not stained by Fe hydroxides (by plain polarized mosaic microscopy image, ViP) when the smallest, least reliable grain fractions (open symbols) are excluded.

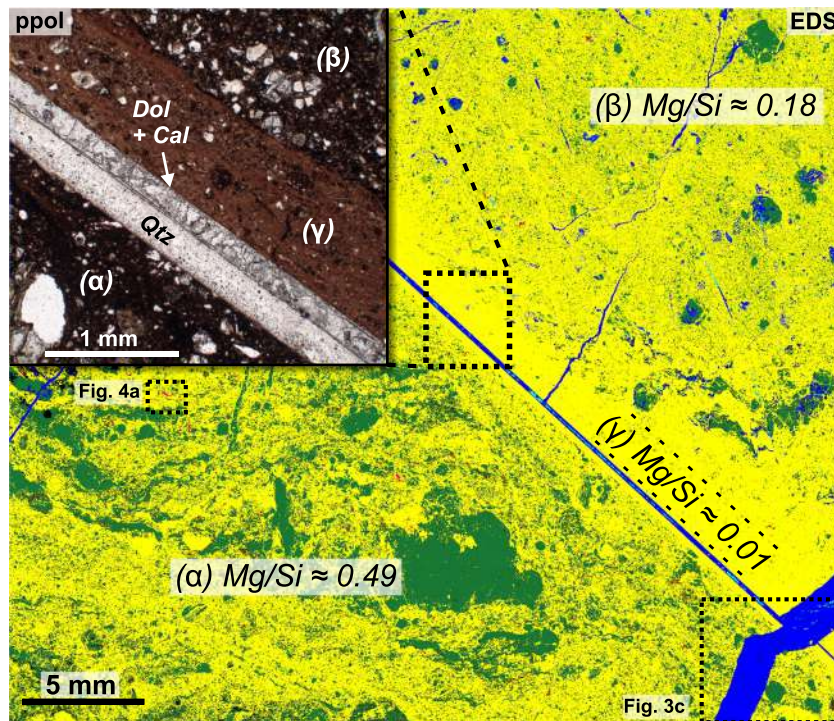


Figure 6. Variation of silica and carbonate contents in reworked cataclastic listvenite. Large area EDS phase map of two cataclasite generations (α and β) separated by an ultracataclasite (γ) and a fault (Sample BT1B_17-2_55-60), showing quartz (yellow), magnesite (green), dolomite (dark blue), calcite (cyan), Fe oxide (red), and Cr-spinel (magenta). The inset in the upper left shows a detail ppol image of the ultracataclasite (γ), and quartz and calcite-dolomite veins along the sharp fault. Average Mg/Si values were calculated using reconstructed EDS spectra integrated over representative areas of the different reworked cataclasite generations.

(γ , Figure 6). A similar, variable enrichment of Si relative to Mg in comparison to the host listvenite is evident in most of the cataclasites we studied in detail (e.g., Figures 7a and 7b). In addition, locally thin (<2 mm) ultracataclastic bands composed of quartz clasts cemented by a Cr-Al-Fe-hydroxide nanoscale phase cut previous cataclasite generations (Figure 7). The nanophase is slightly enriched in Zn and occurs in cataclasite that may contain kaolinite, but where chromian mica is absent. Small clasts of Cr-spinel are similarly abundant in these bands as in other cataclasites. In Sample BT1B_17-2_55-60 thin veins of a similar Cr-Al-Fe hydroxide locally crosscut cataclasite but are truncated by the sharp fault.

Dolomite-cemented breccias occur throughout listvenite in core from Hole BT1B. In macroscopic observation, these can be similar to listvenite cataclasites, with partially rotated, angular fragments of variable grain size. However, EDS chemical mapping revealed that their matrix is consistently composed of dolomite—in contrast to fine-grained quartz and magnesite clasts in cataclasite—and the breccias display a continuous variation in texture, grading into the late dolomite vein network (Figure 8). We interpret these breccias to have formed by overpressured hydrothermal fluid with little tectonic displacement, as opposed to the earlier listvenite cataclasites, which require high strain.

5. Discussion

5.1. Relative Timing of Listvenite Formation and Cataclasis

Cataclastic deformation could in principle provide a positive feedback for the replacement of peridotite by listvenite due to mechanically enhanced reaction rates, if cataclasis was coeval with carbonation (Lisabeth et al., 2017). However, in the case of the thin sections we analyzed, composed of macroscopically well-defined cataclasites of Hole BT1B, the microstructures consistently show that cataclasis occurred in previously formed listvenites. This is shown by truncated clasts of listvenite with spheroidal magnesite, fragments of magnesite and chalcedony-magnesite veins that elsewhere crosscut listvenite, and reworked

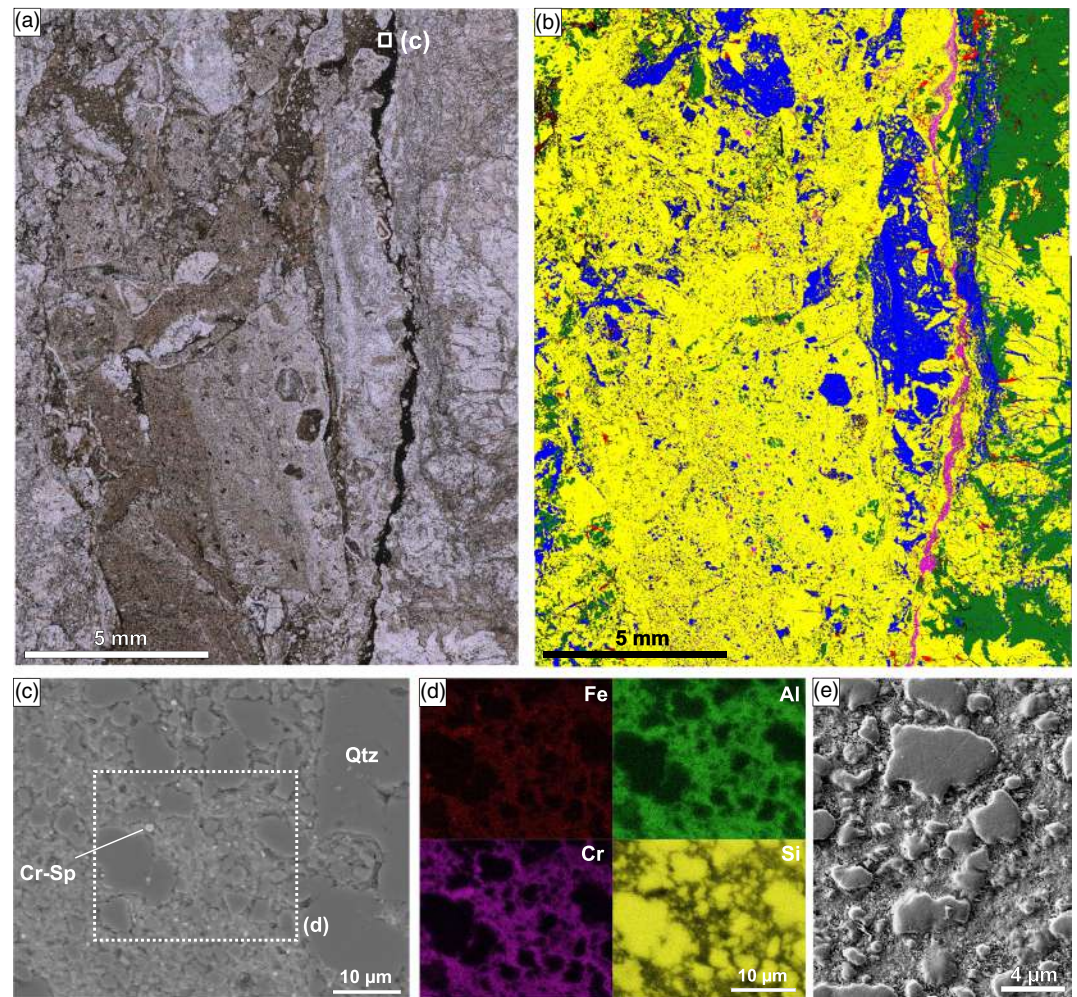


Figure 7. Vertically oriented and multiply reactivated listvenite cataclasite with late, dark ultracataclastic band (Sample BT1B_65-2_22-26). (a) Plain polarized overview (ViP). (b) Phase map from SEM-EDS mapping (yellow = quartz; green = magnesite; blue = dolomite; red = kaolinite/clay; magenta = Cr-rich phases). The cataclasite is reworked and has significantly less magnesite than the host listvenite on the right and left sides of the image. (c) BSE image of dark ultracataclastic band in (a); darker clasts are quartz/silica. (d) EDS chemical maps of area in (c) showing cementation of quartz clasts by an interstitial Cr-Al-Fe nanophase. (e) SE image of quartz μ -clasts cemented by the interstitial Cr-Al-Fe phase.

breccia fragments, all within cataclasites. The observation of truncated growth zonation at the rims of fragmented magnesite clasts (Figure 4b) provides further evidence that cataclasites formed after listvenite formation.

The widespread occurrence of cataclasites throughout listvenites of the core from Hole BT1B, and the common reactivation and reworking of older cataclasites by younger cataclasites and faults, indicates a multi-phase, distributed, brittle, postlistvenite deformation in Hole BT1B, perhaps in a relay zone between larger faults. Our study shows that the most evident records of brittle shear—cataclasites composed of listvenite fragments—formed after the formation of listvenite. Nevertheless, it is possible that earlier examples of cataclasites occur elsewhere in the Oman listvenite and that cataclasis before or during listvenite formation may have been obscured in the core due to subsequent overprint by veins or dissolution-precipitation reactions.

5.2. Fluid Flow and Chemical Modification in Listvenite Cataclasites

SEM-EDS chemical mapping revealed that in most of the studied samples, cataclasites have a significantly lower Mg/Si ratio than the host listvenite, indicating the local dissolution of magnesite and/or addition of

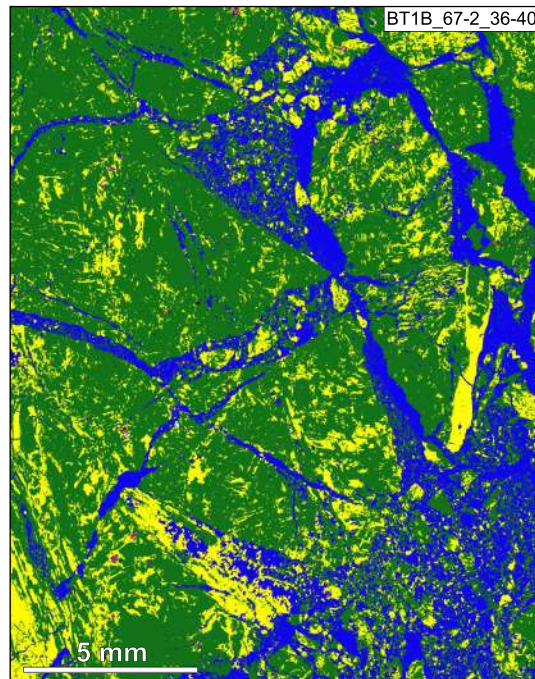


Figure 8. SEM-EDS phase map of dolomite-cemented breccia in listvenite, with quartz (yellow), magnesite (green), dolomite (blue), and Cr-spinel (magenta).

SiO₂. The results show that repeated reactivation and reworking to subsequently finer-grained cataclasite was correlated with increased Mg loss and/or silica enrichment (Figure 6), suggesting that this bulk chemical modification was related to the fluids present during and shortly after cataclastic deformation. Thermodynamic reaction path modeling at relatively low temperatures (100°C) suggests that extremely high fluid/rock ratios could lead to complete carbonate dissolution together with silica enrichment (i.e., birbirite formation) produced by the same fluids that form listvenite at lower fluid/rock ratios (Klein & Garrido, 2011). Because the solubility of silica increases with temperature while that of magnesite decreases, and the thermodynamic models of Klein and Garrido (2011) predict birbirite formation and low pH at 100°C, but not 200°C, 300°C, or 400°C, the observed silica addition and Mg loss in cataclastic listvenite are consistent with the geothermometry constraints to 80–130°C for listvenite formation (Falk & Kelemen, 2015).

Thin, ultracataclastic bands cemented by a Cr-Al-Fe-hydroxide nanophase that represent the last cataclasite generation (Figure 7) likely formed from low pH fluids. At 90°C, experiments and thermodynamic calculations indicate that Cr is ~4 orders of magnitude more soluble in aqueous fluids at pH 4 than at pH 6, whereas it is largely insoluble at neutral and moderately alkaline pH (Rai et al., 1987). Therefore, Cr mobilization in aqueous fluids is incompatible with the slightly alkaline conditions buffered by carbonate dissolution and likely minor in high pH fluids produced by serpentinization (Chavagnac et al., 2013; Giampouras et al., 2020; Paukert et al., 2012). The absence of chromian mica and the presence of kaolinite in the vicinity of ultracataclasite bands cemented by the Cr-Al-Fe-hydroxide nanophase (Figure 7b) is consistent with the higher dissolution rates of mica at lower pH (Pachana et al., 2012), suggesting Cr remobilization due to mica dissolution in addition to chromite alteration. A slightly acidic pH of fluids related to cataclasite cementation is further in agreement with the inferred local carbonate dissolution (Figure 6) and indicates that fluids were out of equilibrium with listvenite during this stage of reaction and deformation. We interpret the observation that Cr-Al-Fe-hydroxide veins are rare, while Cr-spinel fragments are common in cataclasites, to be due to the pH buffer capacity of magnesite dissolution, which prevented larger-scale remobilization of Cr.

The observation that dolomite and dolomite-calcite veins often crosscut cataclasites (Figure 8), breccias, and faults suggests that part of the Ca gain with respect to mantle peridotite, as observed in the Oman listvenites (Falk & Kelemen, 2015; Godard et al., 2017; Kelemen et al., 2017, 2020), may be related to late fluids after the main listvenite formation occurred. Some of the young dolomite and dolomite-calcite may have precipitated from fluid derived from unconformably overlying Tertiary limestone (de Obeso & Kelemen, 2018) or may be of meteoric origin, similar to the widespread surface-near occurrence of carbonate veins and travertine deposits in the Oman peridotites (Giampouras et al., 2020; Noël et al., 2018; Streit et al., 2012). Scharf et al. (2020) report a U/Pb age of 55 ± 4 Ma for calcite veins cutting listvenite near the village of Fanjah, consistent with the hypothesis that fluid flow during Eocene deformation may have redistributed Ca in the listvenites and/or introduced additional Ca from sediments above or below the ophiolite.

5.3. Relationship With Postobduction Tectonics

In the absence of absolute dating of the cataclastic listvenite, three main, protracted tectonic phases could be related to cataclastic deformation of the basal peridotites and listvenites: (i) brittle thrusting during ophiolite obduction (Figure 9a), (ii) postobduction extensional shear zones or reactivation (“retrocharriage”) of previous reverse faults (e.g., Gray & Gregory, 2003) (Figure 9b), and/or (iii) late oblique normal or strike-slip faulting related to uplift of the Jebel Akhdar and Saih Hatat anticlinoria (Figures 9c and 9d).

Ophiolite obduction onto the continental platform was followed by ductile top to the NE shear along listric shear zones, normal to oblique-slip faults of late Cretaceous to early Paleogene age, and subsequent strike-slip faults during the Eocene in limestone (Figures 9b–9d; cf. section 2.1), accompanying the

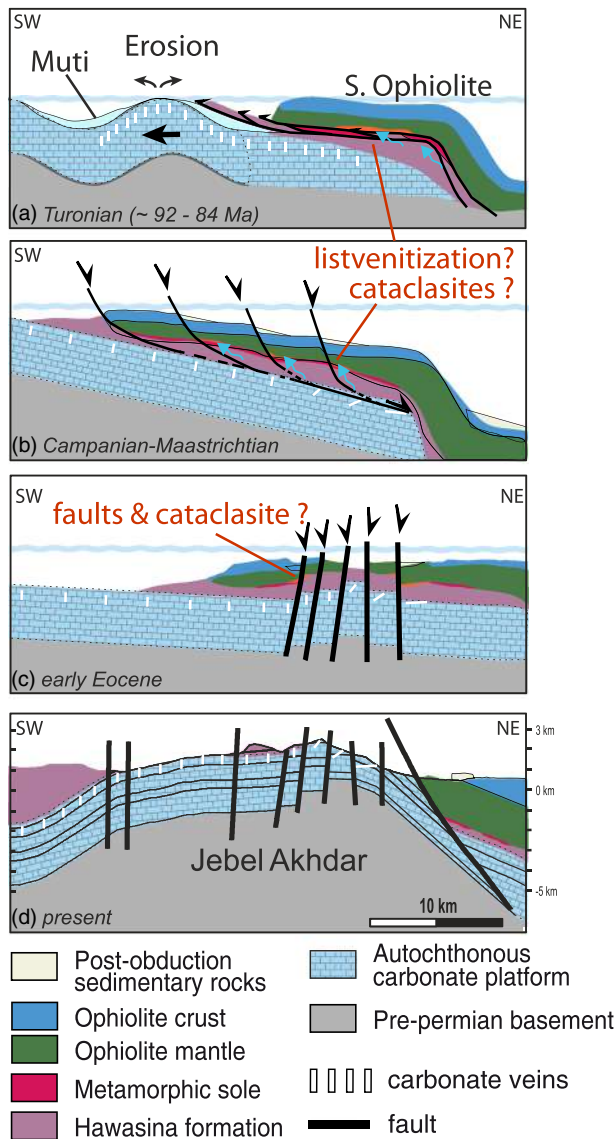


Figure 9. Sketch of the simplified postobduction tectonic evolution of the Samail ophiolite and carbonate platform in Oman (after Grobe et al., 2018), with potential stages of brittle deformation in listvenite at the base of the ophiolite (orange).

exhumation of the autochthonous continental margin in the Jebel Akhdar and Saih Hatat anticlinoria (Gomez-Rivas et al., 2014; Grobe et al., 2018, 2019; Hansman et al., 2018). Because the strength of magnesite is significantly higher than that of calcite limestones (Holyoke et al., 2014), extensional deformation recorded by ductile top to the NE shear zones in the carbonate platform (Figure 9b) may have been related to cataclasis in listvenite, possibly reactivating earlier structures.

Cataclasites could have continued to form during subsequent faulting of the carbonate platform in the early Paleogene to Eocene (Figure 9c), which may be recorded by some of the faults in listvenite and at many of the contacts between listvenite, serpentinite, and the metamorphic sole (Figures 1a and 1c). Calcite-filled microfaults with normal shear sense in the metamorphic sole of Hole BT1B (Kotowski et al., 2020) are possibly related to this stage. The abundance of calcite veins in the Cretaceous section below the ophiolite (Grobe et al., 2018) points to a significant amount of fluid flow during this phase. Fluid inclusion thermometry in quartz and calcite veins in the limestones indicate cooling from about 220–130°C during the transition from normal to strike-slip faulting during exhumation of the Jebel Akhdar (Grobe et al., 2019). In the Saih Hatat, uplift and cooling started somewhat earlier, reaching 120–90°C in the Eocene (Hansman et al., 2017). Reactivation of listvenite cataclasites by sharp faults and the formation of dolomite-cemented breccias in the Wadi Mansah area may be partly related to the uplift of the erosional surface atop the Jebel Akhdar and Saih Hatat anticlinoria to their current high topography (Figure 9d) and the development of the Samail gap fault zone (Scharf et al., 2019).

5.4. Cataclasis—Feedbacks for Carbonation and Carbonate Dissolution

The close spatial relation of listvenites with the basal thrust and other faults in Oman and other ophiolites (Ash & Arksey, 1989; Menzel et al., 2018; Qiu & Zhu, 2018) suggests that the interplay between major tectonic deformation and fluid flux may play a key role in large-scale formation of listvenites. In these settings, cataclasites and dilatant faults and veins are likely to occur, which may enhance reactivity with CO₂-bearing fluids (Lisabeth et al., 2017). Our results demonstrate that cataclasis indeed can enhance fluid flow and chemical reactivity; however, the most evident and widespread cata-

6. Conclusions

1. Visual core logging shows that about 10 vol% of listvenite and serpentinite throughout Hole BT1B has been converted to cataclasite. Continuous core sections >1 m without cataclasites are rare. The width of cataclastic bands in listvenite ranges from <1 mm to >100 cm. Brittle grain size reduction led to a power law grain size distribution in cataclasites with rounded clasts. We interpret this to be formed by multiple phases of movement in an array of small (dm to m scale) faults.
2. In all samples with thin sections of macroscopically identified cataclasites, the microstructures show that cataclasis overprints previously formed listvenites, as indicated by truncated clasts of host listvenite with spheroidal magnesite habit, fragments of chalcedony-magnesite veins, and reworked breccia fragments in cataclasite.
3. Sharp faults, dolomite veins, and dolomite-calcite veins crosscut listvenite cataclasites and are the youngest brittle deformation structures in the core.
4. SEM-EDS chemical mapping reveals that cataclasites commonly have a lower Mg/Si ratio than the host listvenite, indicating the local dissolution of magnesite and/or addition of SiO₂ in cataclasites by reactive fluids.
5. Thin ultracataclastic bands with an interstitial Cr-Al-Fe-hydroxide nanophase are the last cataclasis generation. The mobility of Cr and Al in this process suggests that they formed from acidic aqueous fluids (pH ≤ 4) related to dissolution of magnesite and chromian mica.
6. Repeated brittle overprinting and reactivation of cataclastic listvenite in the field and Hole BT1B core show that there were multiple brittle deformation events postdating listvenite formation in the basal section of the Samial ophiolite. Some or all of this multistage brittle overprint of listvenite by cataclasites, faults, and late veins may be related to the evolution of the sedimentary continental margin units underlying the ophiolite after obduction.
7. Postobduction brittle deformation with related fluid flow and local chemical overprint is likely common in the basal section of the Samail ophiolite, Oman, and should be excluded when analyzing earlier structures to understand the chemomechanical process of listvenite formation.

Acknowledgments

M. D. M. and J. L. U. acknowledge funding by the German Research Foundation (Deutsche Forschungsgemeinschaft [DFG] grant UR 64/20-1). This research used samples and data provided by the Oman Drilling Project. The Oman Drilling Project (OmanDP) has been possible through comingled funds from the International Continental Scientific Drilling Project (ICDP), the Alfred P. Sloan Foundation—Deep Carbon Observatory (Grant 2014-3-01), the U.S. National Science Foundation (NSF-EAR-1516300), the National Aeronautics and Space Administration (NASA)—Astrobiology Institute (NNA15BB02A), the German Research Foundation (DFG: KO 1723/21-1), the Japan Society for the Promotion of Science (JSPS no. 16H06347 and KAKENHI 16H02742), the European Research Council (adv. no. 669972), the Swiss National Science Foundation (Schweizerischer Nationalfonds zur Förderung der wissenschaftlichen Forschung, SNF:20FI21_163073), the Japan Agency for Marine-Earth Science and Technology (JAMSTEC), and the International Ocean Discovery Program (IODP) and contributions from the Sultanate of Oman Ministry of Regional Municipalities and Water Resources, the Oman Public Authority of Mining, Sultan Qaboos University, CRNS-Univ. Montpellier II, Columbia University of New York, and the University of Southampton. We thank the Oman Public Authority of Mining for support to conduct field work and sample export. Werner Kraus and Jonatan Schmidt are thanked for thin section preparation. We are further grateful for editorial handling by Stephen Parman and the suggestions of two anonymous reviewers. Open access funding enabled and organized by Projekt DEAL.

References

- Agar, P., Searle, M. P., Alsop, G. I., & Dubacq, B. (2010). Crustal stacking and expulsion tectonics during continental subduction: P-T deformation constraints from Oman. *Tectonics*, 29, TC5018. <https://doi.org/10.1029/2010TC002669>
- Akbulut, M., Piskin, O., & Karayigit, A. I. (2006). The genesis of the carbonatized and silicified ultramafics known as listvenites: A case study from the Mihalicik region (Eskişehir), NW Turkey. *Geological Journal*, 41(5), 557–580. <https://doi.org/10.1002/gj.1058>
- Alt, J. C., Schwarzenbach, E. M., Früh-Green, G. L., Shanks III, W. C., Bernasconi, S. M., Garrido, C. J., et al. (2013). The role of serpentinites in cycling of carbon and sulfur: Seafloor serpentinization and subduction metamorphism. *Lithos*, 178, 40–54. <https://doi.org/10.1016/j.lithos.2012.12.006>
- Al-Wardi, M., & Butler, R. W. H. (2007). Constrictional extensional tectonics in the northern Oman Mountains, its role in culmination development and the exhumation of the subducted Arabian continental margin. *Geological Society, London, Special Publications*, 272(1), 187. <https://doi.org/10.1144/GSL.SP.2007.272.01.11>
- Andreani, M., Luquot, L., Gouze, P., Godard, M., Hoisé, E., & Gibert, B. (2009). Experimental study of carbon sequestration reactions controlled by the percolation of CO₂-rich brine through peridotites. *Environmental Science & Technology*, 43(4), 1226–1231. <https://doi.org/10.1021/es8018429>
- Ash, C. H., & Arksey, R. L. (1989). The Atlin ultramafic allochthon: Ophiolitic basement within the Cache Creek terrane; tectonic and metallogenic significance. *British Columbia Geological Survey Field Report*, 104N/12.
- Béchenec, F., Roger, J., Le Métour, J., & Wyns, R. (Cartographer). (1992). Geological map, Oman 1: 250,000, Sheet NF40-03, Seeb
- Beinlich, A., Austrheim, H., Mavromatis, V., Grguric, B., Putnis, C. V., & Putnis, A. (2018). Peridotite weathering is the missing ingredient of Earth's continental crust composition. *Nature Communications*, 9(1), 634. <https://doi.org/10.1038/s41467-018-03039-9>
- Beinlich, A., John, T., Vrijmoed, J. C., Tominaga, M., Magna, T., & Podladchikov, Y. Y. (2020). Instantaneous rock transformations in the deep crust driven by reactive fluid flow. *Nature Geoscience*, 13(4), 307–311. <https://doi.org/10.1038/s41561-020-0554-9>
- Beinlich, A., Plümper, O., Boter, E., Müller, I. A., Kourim, F., Ziegler, M., et al. (2020). Ultramafic rock carbonation: Constraints from listvenite core BT1B, Oman Drilling Project. *Journal of Geophysical Research: Solid Earth*, 125, e2019JB019060. <https://doi.org/10.1029/2019JB019060>
- Beinlich, A., Plümper, O., Hövelmann, J., Austrheim, H., & Jamtveit, B. (2012). Massive serpentinite carbonation at Linnajavri, N-Norway. *Terra Nova*, 24(6), 446–455. <https://doi.org/10.1111/j.1365-3121.2012.01083.x>
- Billi, A. (2007). On the extent of size range and power law scaling for particles of natural carbonate fault cores. *Journal of Structural Geology*, 29(9), 1512–1521. <https://doi.org/10.1016/j.jsg.2007.06.007>
- Chavagnac, V., Monnin, C., Ceuleneer, G., Boulart, C., & Hoareau, G. (2013). Characterization of hyperalkaline fluids produced by low-temperature serpentinization of mantle peridotites in the Oman and Ligurian ophiolites. *Geochemistry, Geophysics, Geosystems*, 14, 2496–2522. <https://doi.org/10.1002/ggge.20147>
- Coleman, R. G. (1981). Tectonic setting for ophiolite obduction in Oman. *Journal of Geophysical Research*, 86(B4), 2497–2508. <https://doi.org/10.1029/JB086iB04p02497>

- Cowan, R. J., Searle, M. P., & Waters, D. J. (2014). Structure of the metamorphic sole to the Oman Ophiolite, Sumeini Window and Wadi Tayyin: Implications for ophiolite obduction processes. *Geological Society, London, Special Publications*, 392(1), 155. <https://doi.org/10.1144/SP392.8>
- de Obeso, J. C., & Kelemen, P. B. (2018). Fluid rock interactions on residual mantle peridotites overlain by shallow oceanic limestones: Insights from Wadi Fins, Sultanate of Oman. *Chemical Geology*, 498, 139–149. <https://doi.org/10.1016/j.chemgeo.2018.09.022>
- Escayola, M., Proenza, J., van Staal, C., Rogers, N., & Skulski, T. (2009). The Point Rousse listvenites, Baie Verte, Newfoundland: Altered ultramafic rocks with potential for gold mineralization. Current Research Geological Survey Report, 09-1, 1–12.
- Evans, O., Spiegelman, M., & Kelemen, P. B. (2020). Phase-field modeling of reaction-driven cracking: Determining conditions for extensive olivine serpentinization. *Journal of Geophysical Research: Solid Earth*, 125, e2019JB018614. <https://doi.org/10.1029/2019JB018614>
- Falk, E. S., & Kelemen, P. B. (2015). Geochemistry and petrology of listvenite in the Samail ophiolite, Sultanate of Oman: Complete carbonation of peridotite during ophiolite emplacement. *Geochimica et Cosmochimica Acta*, 160, 70–90. <https://doi.org/10.1016/j.gca.2015.03.014>
- Farough, A., Moore, D. E., Lockner, D. A., & Lowell, R. P. (2016). Evolution of fracture permeability of ultramafic rocks undergoing serpentinization at hydrothermal conditions: An experimental study. *Geochemistry, Geophysics, Geosystems*, 17, 44–55. <https://doi.org/10.1002/2015GC005973>
- Ghent, E. D., & Stout, M. Z. (1981). Metamorphism at the base of the Samail ophiolite, southeastern Oman Mountains. *Journal of Geophysical Research*, 86(B4), 2557–2571. <https://doi.org/10.1029/JB086iB04p02557>
- Giampouras, M., Garrido, C. J., Bach, W., Los, C., Fussmann, D., Monien, P., & García-Ruiz, J. M. (2020). On the controls of mineral assemblages and textures in alkaline springs, Samail Ophiolite, Oman. *Chemical Geology*, 533, 119435. <https://doi.org/10.1016/j.chemgeo.2019.119435>
- Glennie, K. W., Boeuf, M. G. A., Clarke, M. W. H., Moody Stuart, M., Pilaar, W. F. H., & Reinhardt, B. M. (1974). Geology of the Oman Mountains. In *Verhandelingen van het Koninklijk Nederlands Geologisch Mijnbouwkundig Genootschap* (Vol. 31, pp. 1–423). The Hague: Koninklijk Nederlands Geologisch Mijnbouwkundig Genootschap.
- Godard, M., Bennett, E., Carter, E., Kourim, F., Lafay, R., Noël, J., et al. (2017). Geochemical and mineralogical profiles across the listvenite-metamorphic transition in the basal megathrust of the Oman ophiolite: First results from Drilling at Oman Drilling Project Hole BT1B. *AGU Fall Meeting 2017, Abstract V24E-07*.
- Godard, M., Jousset, D., & Bodinier, J.-L. (2000). Relationships between geochemistry and structure beneath a palaeo-spreading centre: A study of the mantle section in the Oman ophiolite. *Earth and Planetary Science Letters*, 180(1–2), 133–148. [https://doi.org/10.1016/S0012-821X\(00\)00149-7](https://doi.org/10.1016/S0012-821X(00)00149-7)
- Godard, M., Luquot, L., Andreani, M., & Gouze, P. (2013). Incipient hydration of mantle lithosphere at ridges: A reactive-percolation experiment. *Earth and Planetary Science Letters*, 371–372, 92–102. <https://doi.org/10.1016/j.epsl.2013.03.052>
- Gomez-Rivas, E., Bons, P. D., Koehn, D., Urai, J. L., Arndt, M., Virgo, S., et al. (2014). The Jabal Akhdar dome in the Oman Mountains: Evolution of a dynamic fracture system. *American Journal of Science*, 314(7), 1104–1139. <https://doi.org/10.2475/07.2014.02>
- Gray, D. R., & Gregory, R. T. (2003). Ophiolite obduction and the Samail Ophiolite: the behaviour of the underlying margin. *Geological Society, London, Special Publications*, 218(1), 449–465. <https://doi.org/10.1144/gsl.sp.2003.218.01.23>
- Grobe, A., Urai, J. L., Littke, R., & Lünsdorf, N. K. (2016). Hydrocarbon generation and migration under a large overthrust: The carbonate platform under the Semail Ophiolite, Jebel Akhdar, Oman. *International Journal of Coal Geology*, 168, 3–19. <https://doi.org/10.1016/j.coal.2016.02.007>
- Grobe, A., Virgo, S., von Hagke, C., Urai, J. L., & Littke, R. (2018). Multiphase structural evolution of a continental margin during obduction orogeny: Insights from the Jebel Akhdar Dome, Oman Mountains. *Tectonics*, 37, 888–913. <https://doi.org/10.1002/2016TC004442>
- Grobe, A., von Hagke, C., Littke, R., Dunkl, I., Wübbeler, F., Muchez, P., & Urai, J. L. (2019). Tectono-thermal evolution of Oman's Mesozoic passive continental margin under the obducting Semail Ophiolite: A case study of Jebel Akhdar, Oman. *Solid Earth*, 10(1), 149–175. <https://doi.org/10.5194/se-10-149-2019>
- Guilmette, C., Smit, M. A., van Hinsbergen, D. J. J., Gürer, D., Corfu, F., Charette, B., et al. (2018). Forced subduction initiation recorded in the sole and crust of the Semail Ophiolite of Oman. *Nature Geoscience*, 11(9), 688–695. <https://doi.org/10.1038/s41561-018-0209-2>
- Hacker, B. R., & Mosenfelder, J. L. (1996). Metamorphism and deformation along the emplacement thrust of the Samail ophiolite, Oman. *Earth and Planetary Science Letters*, 144(3–4), 435–451. [https://doi.org/10.1016/S0012-821X\(96\)00186-0](https://doi.org/10.1016/S0012-821X(96)00186-0)
- Hacker, B. R., Mosenfelder, J. L., & Gnos, E. (1996). Rapid emplacement of the Oman ophiolite: Thermal and geochronologic constraints. *Tectonics*, 15(6), 1230–1247. <https://doi.org/10.1029/96TC01973>
- Halls, C., & Zhao, R. (1995). Listvenite and related rocks: Perspectives on terminology and mineralogy with reference to an occurrence at Cregganbaun, Co. Mayo, Republic of Ireland. *Mineralium Deposita*, 30(3–4), 303–313. <https://doi.org/10.1007/BF00196366>
- Hanghøj, K., Kelemen, P. B., Hassler, D., & Godard, M. (2010). Composition and genesis of depleted mantle peridotites from the Wadi Tayin Massif, Oman Ophiolite; major and trace element geochemistry, and Os isotope and PGE systematics. *Journal of Petrology*, 51(1–2), 201–227. <https://doi.org/10.1093/petrology/egp077>
- Hansen, L. D., Dipple, G. M., Gordon, T. M., & Kellett, D. A. (2005). Carbonated serpentinite (listwanite) at Atlin, British Columbia: A geological analogue to carbon dioxide sequestration. *Canadian Mineralogist*, 43(1), 225–239. <https://doi.org/10.2113/gscanmin.43.1.225>
- Hansman, R. J., Albert, R., Gerdes, A., & Ring, U. (2018). Absolute ages of multiple generations of brittle structures by U-Pb dating of calcite. *Geology*, 46(3), 207–210. <https://doi.org/10.1130/G39822.1>
- Hansman, R. J., Ring, U., Thomson, S. N., den Brok, B., & Stübner, K. (2017). Late Eocene uplift of the Al Hajar Mountains, Oman, supported by stratigraphy and low-temperature thermochronology. *Tectonics*, 36, 3081–3109. <https://doi.org/10.1002/2017TC004672>
- Holyoke, C. W., Kronenberg, A. K., Newman, J., & Ulrich, C. (2014). Rheology of magnesite. *Journal of Geophysical Research: Solid Earth*, 119, 6534–6557. <https://doi.org/10.1002/2013JB010541>
- Hopson, C. A., Coleman, R. G., Gregory, R. T., Pallister, J. S., & Bailey, E. H. (1981). Geologic section through the Samail Ophiolite and associated rocks along a Muscat-Ibra Transect, southeastern Oman Mountains. *Journal of Geophysical Research*, 86(B4), 2527–2544. <https://doi.org/10.1029/JB086iB04p02527>
- Hövelmann, J., Austrheim, H., & Jamtveit, B. (2013). Microstructure and porosity evolution during experimental carbonation of a natural peridotite. *Chemical Geology*, 334, 254–265. <https://doi.org/10.1016/j.chemgeo.2012.10.025>
- Hyndman, R. D., & Peacock, S. M. (2003). Serpentinization of the forearc mantle. *Earth and Planetary Science Letters*, 212(3–4), 417–432. [https://doi.org/10.1016/s0012-821x\(03\)00263-2](https://doi.org/10.1016/s0012-821x(03)00263-2)
- Jöns, N., & Bach, W. (2013). Serpentinization. In J. Harff, M. Meschede, S. Petersen, J. Thiede (Eds.), *Encyclopedia of marine geosciences* (pp. 1–12). Dordrecht: Springer Netherlands.

- Kelemen, P., Godard, M., Johnson, K. T. M., Okazaki, K., Manning, C. E., Urai, J. L., et al. (2017). Peridotite carbonation at the leading edge of the mantle wedge: OmDP Site BT1. *AGU Fall Meeting, Abstract V24E-06*.
- Kelemen, P. B., Aines, R., Bennett, E., Benson, S. M., Carter, E., Coggon, J. A., et al. (2018). In situ carbon mineralization in ultramafic rocks: Natural processes and possible engineered methods. *Energy Procedia*, *146*, 92–102. <https://doi.org/10.1016/j.egypro.2018.07.013>
- Kelemen, P. B., & Hirth, G. (2012). Reaction-driven cracking during retrograde metamorphism: Olivine hydration and carbonation. *Earth and Planetary Science Letters*, *345–348*(supplement C), 81–89. <https://doi.org/10.1016/j.epsl.2012.06.018>
- Kelemen, P. B., & Manning, C. E. (2015). Reevaluating carbon fluxes in subduction zones, what goes down, mostly comes up. *Proceedings of the National Academy of Sciences*, *112*(30), E3997–E4006. <https://doi.org/10.1073/pnas.1507889112>
- Kelemen, P. B., & Matter, J. M. (2008). In situ carbonation of peridotite for CO₂ storage. *Proceedings of the National Academy of Sciences*, *105*(45), 17,295–17,300. <https://doi.org/10.1073/pnas.0805794105>
- Kelemen, P. B., Matter, J. M., Streit, E. E., Rudge, J. F., Curry, W. B., & Blusztajn, J. (2011). Rates and mechanisms of mineral carbonation in peridotite: Natural processes and recipes for enhanced, in situ CO₂ capture and storage. In R. Jeanloz & K. H. Freeman (Eds.), *Annual Review of Earth and Planetary Sciences*, Vol 39 (pp. 545–576).
- Kelemen, P. B., Matter, J. M., Teagle, D. A. H., Coggon, J. A., & the Oman Drilling Project Science Team (2020). Site BT1: Fluid and mass exchange on a subduction zone plate boundary. In P. B. Kelemen, J. M. Matter, D. A. H. Teagle, J. A. Coggon, the Oman Drilling Project Science Team (Eds.), *Proceedings of the Oman Drilling Project*, MS OmanDP–113, 1–122. College Station, TX: International Ocean Discovery Program. <https://doi.org/10.14379/OmanDP.proc.2020>
- Keulen, N., Stünitz, H., & Heilbronner, R. (2008). Healing microstructures of experimental and natural fault gouge. *Journal of Geophysical Research*, *113*, B06205. <https://doi.org/10.1029/2007JB005039>
- Klein, F., & Garrido, C. J. (2011). Thermodynamic constraints on mineral carbonation of serpentinized peridotite. *Lithos*, *126*(3–4), 147–160. <https://doi.org/10.1016/j.lithos.2011.07.020>
- Klein, F., Grozeva, N. G., Seewald, J. S., McCollom, T. M., Humphris, S. E., Moskowitz, B., et al. (2015). Experimental constraints on fluid-rock reactions during incipient serpentinization of harzburgite. *American Mineralogist*, *100*(4), 991–1002. <https://doi.org/10.2138/am-2015-5112>
- Kotowski, A., Cloos, M., Bos Orent, E., & Stockli, D. (2020). Structural and petrologic evolution of an infant subduction shear zone: Insights from sub-ophiolite metamorphic rocks recovered from the Oman Drilling Project (Hole BT-1B). Proceedings of the International Conference on Ophiolites and Oceanic Lithosphere, 12–14 January, Sultan Qaboos University, Oman, 2020, pages 124–126.
- Lacinska, A. M., & Styles, M. T. (2013). Silicified serpentinite—A residuum of a Tertiary palaeo-weathering surface in the United Arab Emirates. *Geological Magazine*, *150*(3), 385–395. <https://doi.org/10.1017/S0016756812000325>
- Lafay, R., Godard, M., Menzel, M., Beinlich, A., Kourim, F., Decrausaz, T., & the Oman Drilling Project Phase 1 Science Party. (2020). Listvenization processes in the mantle atop the Samail ophiolite metamorphic sole: Mineralogical and thermodynamic constraints. Proceedings of the International Conference on Ophiolites and Oceanic Lithosphere, 12–14 January, Sultan Qaboos University, Oman, 2020, page 129.
- Laurich, B., Urai, J. L., Vollmer, C., & Nussbaum, C. (2018). Deformation mechanisms and evolution of the microstructure of gouge in the Main Fault in Opalinus Clay in the Mont Terri rock laboratory (CH). *Solid Earth*, *9*(1), 1–24. <https://doi.org/10.5194/se-9-1-2018>
- Li, J., & Hitch, M. (2018). Mechanical activation of magnesium silicates for mineral carbonation, a review. *Minerals Engineering*, *128*, 69–83. <https://doi.org/10.1016/j.mineng.2018.08.034>
- Lisabeth, H. P., Zhu, W., Kelemen, P. B., & Ilgen, A. (2017). Experimental evidence for chemo-mechanical coupling during carbon mineralization in ultramafic rocks. *Earth and Planetary Science Letters*, *474*(Supplement C), 355–367. <https://doi.org/10.1016/j.epsl.2017.06.045>
- Macdonald, A. H., & Fyfe, W. S. (1985). Rate of serpentinization in seafloor environments. *Tectonophysics*, *116*(1–2), 123–135. [https://doi.org/10.1016/0040-1951\(85\)90225-2](https://doi.org/10.1016/0040-1951(85)90225-2)
- Malthe-Sørenssen, A., Jamtveit, B., & Meakin, P. (2006). Fracture patterns generated by diffusion controlled volume changing reactions. *Physical Review Letters*, *96*(24), 245501. <https://doi.org/10.1103/PhysRevLett.96.245501>
- Malvoisin, B., Auzande, A. L., Kelemen, P. B., & the Oman Drilling Project Science Party (2020). The mechanism of fluid pathway preservation during solid volume increase in serpentinization. *Geology*.
- Manning, C. E., Kelemen, P. B., Michibayashi, K., Harris, M., Urai, J. L., de Obeso, J. C., et al. (2017). Transformation of serpentinite to listvenite as recorded in the vein history of rocks from Oman Drilling Project Hole BT1B. *AGU Fall Meeting, Abstract V24E-08*.
- Menzel, M. D., Garrido, C. J., López Sánchez-Vizcaíno, V., Marchesi, C., Hidas, K., Escayola, M. P., & Delgado Huertas, A. (2018). Carbonation of mantle peridotite by CO₂-rich fluids: The formation of listvenites in the Advocate ophiolite complex (Newfoundland, Canada). *Lithos*, *323*, 238–261. <https://doi.org/10.1016/j.lithos.2018.06.001>
- Miller, J. M., Gregory, R. T., Gray, D. R., & Foster, D. A. (1999). Geological and geochronological constraints on the exhumation of a high-pressure metamorphic terrane, Oman. *Geological Society, London, Special Publications*, *154*(1), 241. <https://doi.org/10.1144/GSL.SP.1999.154.01.11>
- Monnier, C., Girardeau, J., Le Mée, L., & Polvé, M. (2006). Along-ridge petrological segmentation of the mantle in the Oman ophiolite. *Geochemistry, Geophysics, Geosystems*, *7*, Q11008. <https://doi.org/10.1029/2006GC001320>
- Nasir, S., Al Sayigh, A. R., Al Harthy, A., Al-Khribash, S., Al-Jaaidi, O., Musllam, A., et al. (2007). Mineralogical and geochemical characterization of listwaenite from the Semail Ophiolite, Oman. *Geochemistry*, *67*(3), 213–228. <https://doi.org/10.1016/j.chemer.2005.01.003>
- Nicolas, A., & Boudier, F. (1995). Mapping oceanic ridge segments in Oman ophiolite. *Journal of Geophysical Research*, *100*(B4), 6179–6197. <https://doi.org/10.1029/94JB01188>
- Nicolas, A., Boudier, F., & Ildefonse, B. (1996). Variable crustal thickness in the Oman ophiolite: Implication for oceanic crust. *Journal of Geophysical Research*, *101*(B8), 17,941–17,950. <https://doi.org/10.1029/96JB00195>
- Noël, J., Godard, M., Olliot, E., Martinez, I., Williams, M., Boudier, F., et al. (2018). Evidence of polygenetic carbon trapping in the Oman Ophiolite: Petro-structural, geochemical, and carbon and oxygen isotope study of the Wadi Dima harzburgite-hosted carbonates (Wadi Tayin massif, Sultanate of Oman). *Lithos*, *323*, 218–237. <https://doi.org/10.1016/j.lithos.2018.08.020>
- Nolan, S. C., Skelton, P. W., Clissold, B. P., & Smewing, J. D. (1990). Maastrichtian to early Tertiary stratigraphy and palaeogeography of the Central and Northern Oman Mountains. *Geological Society, London, Special Publications*, *49*(1), 495. <https://doi.org/10.1144/GSL.SP.1992.049.01.31>
- Oelkers, E. H., Declercq, J., Saldi, G. D., Gislason, S. R., & Schott, J. (2018). Olivine dissolution rates: A critical review. *Chemical Geology*, *500*, 1–19. <https://doi.org/10.1016/j.chemgeo.2018.10.008>
- O’Hanley, D. S. (1992). Solution to the volume problem in serpentinization. *Geology*, *20*(8), 705. [https://doi.org/10.1130/0091-7613\(1992\)020<0705:stvpvi>2.3.co;2](https://doi.org/10.1130/0091-7613(1992)020<0705:stvpvi>2.3.co;2)

- Pachana, K., Zuddas, P., & Censi, P. (2012). Influence of pH and temperature on the early stage of mica alteration. *Applied Geochemistry*, 27(9), 1738–1744. <https://doi.org/10.1016/j.apgeochem.2012.02.009>
- Passchier, C. W., & Trouw, R. A. J. (2005). *Microtectonics* (2nd ed.). Berlin Heidelberg New York: Springer.
- Paukert, A. N., Matter, J. M., Kelemen, P. B., Shock, E. L., & Havig, J. R. (2012). Reaction path modeling of enhanced in situ CO₂ mineralization for carbon sequestration in the peridotite of the Samail Ophiolite, Sultanate of Oman. *Chemical Geology*, 330–331, 86–100. <https://doi.org/10.1016/j.chemgeo.2012.08.013>
- Peuble, S., Andreani, M., Godard, M., Gouze, P., Barou, F., Van de Moortele, B., et al. (2015). Carbonate mineralization in percolated olivine aggregates: Linking effects of crystallographic orientation and fluid flow. *American Mineralogist*, 100(2–3), 474–482. <https://doi.org/10.2138/am-2015-4913>
- Peuble, S., Andreani, M., Gouze, P., Pollet-Villard, M., Reynard, B., & Van de Moortele, B. (2018). Multi-scale characterization of the incipient carbonation of peridotite. *Chemical Geology*, 476(Supplement C), 150–160. <https://doi.org/10.1016/j.chemgeo.2017.11.013>
- Plümper, O., Røyne, A., Magrasó, A., & Jamtveit, B. (2012). The interface-scale mechanism of reaction-induced fracturing during serpentinization. *Geology*, 40(12), 1103–1106. <https://doi.org/10.1130/G33390.1>
- Qiu, T., & Zhu, Y. (2018). Listwaenite in the Sartohay ophiolitic mélange (Xinjiang, China): A genetic model based on petrology, U-Pb chronology and trace element geochemistry. *Lithos*, 302–303, 427–446. <https://doi.org/10.1016/j.lithos.2018.01.029>
- Rai, D., Sass, B. M., & Moore, D. A. (1987). Chromium(III) hydrolysis constants and solubility of chromium(III) hydroxide. *Inorganic Chemistry*, 26(3), 345–349. <https://doi.org/10.1021/ic00250a002>
- Rajendran, S., Nasir, S., Kusky, T. M., Ghulam, A., Gabr, S., & El-Ghali, M. A. K. (2013). Detection of hydrothermal mineralized zones associated with listwaenites in Central Oman using ASTER data. *Ore Geology Reviews*, 53, 470–488. <https://doi.org/10.1016/j.oregeorev.2013.02.008>
- Rioux, M., Bowring, S., Kelemen, P., Gordon, S., Miller, R., & Dudás, F. (2013). Tectonic development of the Samail ophiolite: High-precision U-Pb zircon geochronology and Sm-Nd isotopic constraints on crustal growth and emplacement. *Journal of Geophysical Research: Solid Earth*, 118, 2085–2101. <https://doi.org/10.1002/jgrb.50139>
- Rudge, J. F., Kelemen, P. B., & Spiegelman, M. (2010). A simple model of reaction-induced cracking applied to serpentinization and carbonation of peridotite. *Earth and Planetary Science Letters*, 291(1–4), 215–227. <https://doi.org/10.1016/j.epsl.2010.01.016>
- Saddiqi, O., Michard, A., Goffe, B., Poupeau, G. r., & Oberhänsli, R. (2006). Fission-track thermochronology of the Oman Mountains continental windows, and current problems of tectonic interpretation. *Bulletin de la Société Géologique de France*, 177(3), 127–134. <https://doi.org/10.2113/gssgfbull.177.3.127>
- Scharf, A., Mattern, F., Bolhar, R., Bailey, C. M., Ring, U. (2020). U-Pb dating of postobductional carbonate veins in listwaenite of the Oman Mountains near Fanja. Proceedings of the International Conference on Ophiolites and Oceanic Lithosphere, 12–14th January, 2020, Sultan Qaboos University, Muscat, Sultanate of Oman, page 220.
- Scharf, A., Mattern, F., Moraetis, D., Callegari, I., & Weidle, C. (2019). Postobductional kinematic evolution and geomorphology of a major regional structure—The Semail Gap Fault Zone (Oman Mountains). *Tectonics*, 38, 2756–2778. <https://doi.org/10.1029/2019TC005588>
- Searle, M., & Cox, J. (1999). Tectonic setting, origin, and obduction of the Oman ophiolite. *GSA Bulletin*, 111(1), 104–122. [https://doi.org/10.1130/0016-7606\(1999\)111<0104:TSAOO>2.3.CO;2](https://doi.org/10.1130/0016-7606(1999)111<0104:TSAOO>2.3.CO;2)
- Searle, M. P., Waters, D. J., Martin, H. N., & Rex, D. C. (1994). Structure and metamorphism of blueschist–eclogite facies rocks from the northeastern Oman Mountains. *Journal of the Geological Society*, 151(3), 555–576. <https://doi.org/10.1144/gsjgs.151.3.0555>
- Soret, M., Agard, P., Dubacq, B., Plunder, A., & Yamato, P. (2017). Petrological evidence for stepwise accretion of metamorphic soles during subduction infancy (Semail ophiolite, Oman and UAE). *Journal of Metamorphic Geology*, 35(9), 1051–1080. <https://doi.org/10.1111/jmg.12267>
- Soret, M., Bonnet, G., Larson, K., Agard, P., Cottle, J., Dubacq, B., Button, M. (2020). Slow subduction initiation forces fast ophiolite formation. Proceedings of the International Conference on Ophiolites and the Oceanic Lithosphere: Results of the Oman Drilling Project and Related Research 12–14th, Sultan Qaboos University, Muscat, Sultanate of Oman, page 234.
- Stanger, G. (1985). Silicified serpentinite in the Semail nappe of Oman. *Lithos*, 18, 13–22. [https://doi.org/10.1016/0024-4937\(85\)90003-9](https://doi.org/10.1016/0024-4937(85)90003-9)
- Streit, E., Kelemen, P., & Eiler, J. (2012). Coexisting serpentine and quartz from carbonate-bearing serpentinized peridotite in the Samail Ophiolite, Oman. *Contributions to Mineralogy and Petrology*, 164(5), 821–837. <https://doi.org/10.1007/s00410-012-0775-z>
- Tutolo, B. M., Mildner, D. F. R., Gagnon, C. V. L., Saar, M. O., & Seyfried, W. E. Jr. (2016). Nanoscale constraints on porosity generation and fluid flow during serpentinization. *Geology*, 44(2), 103–106. <https://doi.org/10.1130/G37349.1>
- Ulven, O. I., Storheim, H., Austrheim, H., & Malthe-Sørenssen, A. (2014). Fracture initiation during volume increasing reactions in rocks and applications for CO₂ sequestration. *Earth and Planetary Science Letters*, 389, 132–142. <https://doi.org/10.1016/j.epsl.2013.12.039>
- van Noort, R., Wolterbeek, T. K. T., Drury, M. R., Kandianis, M. T., & Spiers, C. J. (2017). The force of crystallization and fracture propagation during in-situ carbonation of peridotite. *Minerals*, 7(10), 190. <https://doi.org/10.3390/min7100190>
- Villey, M., Le Métour, J., & de Gramont, X. (1986). Geological map of Fanjah. Bureau de Recherches Géologiques et Minières (BRGM), Orléans, France; Muscat, Oman, Ministry of Petroleum and Minerals, Directorate General of Minerals, Sultanate of Oman.
- Virgo, S., Arndt, M., Sobisch, Z., & Urai, J. L. (2013). Development of fault and vein networks in a carbonate sequence near Hayl al-Shaz, Oman Mountains. *GeoArabia*, 18(2), 99–136.
- Virgo, S., Heup, T., Urai, J. L., & Berlageet, T. (2016). Virtual petrography (ViP)—A virtual microscope for the geosciences. *Geophysical Research Abstracts*, 18, EGU2016–14669–1 <http://meetingorganizer.copernicus.org/EGU2016/EGU2016-14669-1.pdf>
- Wilde, A., Simpson, L., & Hanna, S. (2002). Preliminary study of Cenozoic hydrothermal alteration and platinum deposition in the Oman Ophiolite. *Journal of the Virtual Explorer*, 6, 7–13.
- Xing, T., Zhu, W., Fousseis, F., & Lisabeth, H. (2018). Generating porosity during olivine carbonation via dissolution channels and expansion cracks. *Solid Earth*, 9(4), 879–896. <https://doi.org/10.5194/se-9-879-2018>
- Zheng, X., Cordonnier, B., Zhu, W., Renard, F., & Jamtveit, B. (2018). Effects of confinement on reaction-induced fracturing during hydration of periclase. *Geochemistry, Geophysics, Geosystems*, 19, 2661–2672. <https://doi.org/10.1029/2017GC007322>
- Zhu, W., Fousseis, F., Lisabeth, H., Xing, T., Xiao, X., De Andrade, V., & Karato, S.-I. (2016). Experimental evidence of reaction-induced fracturing during olivine carbonation. *Geophysical Research Letters*, 43, 9535–9543. <https://doi.org/10.1002/2016GL070834>